Research Square

Preprints are preliminary reports that have not undergone peer review.
They should not be considered conclusive, used to inform clinical practice,
or referenced by the media as validated information.

Antibiotic-induced gut dysbiosis triggers systemic metabolic reprogramming via depletion of microbiota-derived tryptophan metabolites in broilers

Juanjuan Xiong
Jinling Institute of Technology
Baofeng Chen
Jinling Institute of Technology
Hui Wang
Jinling Institute of Technology
Xinjie Bai
80602@bvca.edu.cn
Beijing Vocational College of Agriculture

Research Article

Keywords: Antibiotic cocktail, Gut microbiota, Tryptophan metabolism, Metabolomics, Broiler

Posted Date: November 12th, 2026

DOI: https://doi.org/10.21203/rs.3.rs-11137923/v1

License: This work is licensed under a Creative Commons Attribution 4.0 International License.
Read Full License

Additional Declarations: No competing interests reported.

Antibiotic-induced gut dysbiosis triggers systemic metabolic reprogramming via depletion of microbiota-derived tryptophan metabolites in broilers

Juanjuan Xiong [1], Baofeng Chen [1], Hui Wang [1], Xinjie Bai [2*]

[1] College of Animal Science and Food Engineering, Jinling Institute of Technology, Qixia, Nanjing 210046, China

[2] College of Animal Science and Technology, Beijing Vocational College of Agriculture, Beijing 102442, China

Scientific section: Gut microbiome health

Text pages: 32

Table: 1

Figures: 6

Correspondence should be addressed to

Xinjie Bai

College of Animal Science and Technology, Beijing Vocational College of Agriculture, Beijing 102442, China

E-mail: 80602@bvca.edu.cn

Tel.: 15652767380

Abstract

Background The poultry industry has widely used antibiotics at growth-promoting doses, a practice that has accelerated antimicrobial resistance. However, the effects of prolonged low-dose antibiotic exposure on chicken gut microbiota and systemic metabolism remain inadequately understood.

Results Broilers received a broad-spectrum antibiotic cocktail in drinking water, and 16S rRNA sequencing, serum metabolomics, and phenotypic measurements were integrated to investigate antibiotic impacts on the gut microbiota and mechanisms of metabolic regulation. Antibiotic treatment significantly altered the cecal microbial community, marked by reductions in *Lactobacillus* and butyrate-producing genera and increases in *Escherichia-Shigella* and *Enterococcus*(P<0.05). Functional gene prediction indicated downregulation of carbohydrate and amino acid metabolism pathways alongside upregulation of ABC transporters and quorum sensing systems. Consistent with this functional shift, tryptophan-derived indole metabolites were the most depleted class of circulating metabolites: 5-hydroxyindoxyl sulfate, quinoline 1-oxide and 2,8-quinolinediol were each reduced by 45–53%. Their depletion was accompanied by broad host metabolic remodeling, including significant increases in branched-chain amino acid catabolites , a coordinated reduction of six phospholipid species (FDR < 0.05) with lysophosphatidylcholines declining most consistently, elevated markers of oxidative stress and of antioxidant defense. Trends toward increased fatty acid oxidation and impaired TCA cycle flux were also observed. These

metabolic alterations were accompanied by reduced intestinal length and lower immune organ indices.

Conclusions Long-term exposure to a broad-spectrum antibiotic cocktail induces gut dysbiosis and depletes microbiota-derived tryptophan – indole metabolites, which is accompanied by systemic metabolic remodeling and impaired intestinal and organ development in broilers. These findings identify microbial tryptophan metabolism as a candidate target for mitigating antibiotic-induced metabolic impairment.

Keywords: Antibiotic cocktail, Gut microbiota, Tryptophan metabolism, Metabolomics, Broiler

1 Introduction

Since the discovery that certain antibiotics at sub-therapeutic doses can promote growth in chickens, they have been widely used in poultry production to improve feed conversion efficiency and enhance growth performance. These compounds are collectively referred to as antibiotic growth promoters (AGPs)[1]. The growth-promoting mechanisms of AGPs have been partially elucidated; for instance, they may promote growth by reshaping the gut microbial community structure and thereby altering the host's efficiency in nutrient utilization[2].

The use of antibiotics as growth promoters in poultry remains controversial [3]. Some reports indicate that broilers fed AGP-supplemented diets show higher weight gain and better feed conversion rates compared to controls, whereas withdrawal of AGPs increases production costs [4]. Low-dose antibiotics have also been shown to

enhance intestinal barrier function, improve feed conversion efficiency, and exert growth-promoting effects [3,5]. However, other studies report that exposure to low-dose penicillin can persistently disrupt gut microbiota and exacerbate diet-induced metabolic disorders [6]. Although antibiotic administration can initially reduce pathogenic bacterial abundance during treatment, withdrawal leads to a rebound of pathogens such as Alloprevotella and an increase in other pathogenic taxa like Oscillibacter [7]. Moreover, continued antibiotic use promotes dissemination of resistance genes within the gut microbiome, leading to the emergence of multidrug-resistant bacteria and posing significant threats to animal health and food safety [8,9]. Despite growing attention to long-term low-dose antibiotic exposure, its impact on gut microbiota remains insufficiently investigated, and the consequences for poultry health warrant further exploration.

The gut microbiota facilitates the breakdown of dietary carbohydrates, synthesizes essential vitamins and amino acids, and produces bioactive metabolites—including short-chain fatty acids (SCFAs), bile acid derivatives, and tryptophan catabolites—that support host immune homeostasis, intestinal barrier integrity, and systemic metabolic balance [10,11]. When microbial metabolic capacity is compromised, the risk of inflammatory and metabolic diseases rises substantially [10,12]. Among these metabolites, SCFAs have attracted considerable attention because they not only regulate intestinal health but also directly or indirectly influence immune function at extra-intestinal sites (such as the liver, lungs, reproductive tract, and brain) and are linked to various diseases [13,14]. Research on tryptophan

metabolites has largely centered on the gut–brain axis [15]. Recently, accumulating evidence shows that microbiota-derived indole derivatives from tryptophan metabolism promote intestinal barrier integrity and immune development[16,17]. However, it remains unclear which specific metabolites primarily mediate the effects of gut microbial alterations on systemic metabolic homeostasis in broilers after long-term, low-dose antibiotic exposure.

To simulate continuous disruption of the gut microbiota by antibiotic exposure in poultry production, this study established a model using a low-dose antibiotic combination to broadly perturb the intestinal microbiota. We systematically investigated how these microbial alterations affect host systemic metabolism and evaluated their impact on growth performance, aiming to provide a theoretical basis for comprehensively understanding the effects and risks of sub-therapeutic antibiotic use.

2 Materials and Methods

2.1 Animal experimental design

A total of 36 healthy Arbor Acres (AA) broilers were purchased from a local commercial farm (Tegeili Planting Cooperative) in Nanjing, China, and randomly assigned to two groups (n = 18 per group): a control group and an antibiotic-treated group. The control group received normal feed and drinking water, while the antibiotic group received drinking water supplemented with an antibiotic cocktail of penicillin (100 mg/L), neomycin (100 mg/L), metronidazole (100 mg/L), and

streptomycin (50 mg/L). This broad-spectrum combination was used to deplete the gut microbiota. All animal experiments in this study were reviewed and approved by the Ethics Committee of the College of Animal Science and Food Engineering, Jinling Institute of Technology (Approval Date:October 23, 2025). All procedures were performed in compliance with international, national, and institutional guidelines for the care and use of animals, and were reported in accordance with the ARRIVE guidelines. Every effort was made to minimize animal suffering and distress.

Broilers were reared from day 0 and sampled on days 14, 21, and 35. At each sampling time point, broilers were euthanized by cervical dislocation. Death was confirmed by observing cessation of heartbeat. Body weight was recorded, and organs including the liver, spleen, thymus, and bursa of Fabricius were weighed to calculate organ indices (organ weight/body weight × 100). The lengths of intestinal segments (duodenum, jejunum, ileum, and colorectum) were measured. On day 35, blood samples were collected from the heart, centrifuged at 3,000 rpm for 15 minutes at 4°C, and serum was stored at −80°C for metabolomic analysis. Cecal contents were collected immediately, snap-frozen in liquid nitrogen, and stored at −80°C for 16S rRNA sequencing.

2.2 DNA extraction and 16S rRNA sequencing

Total genomic DNA of the microbial community was extracted using the E.Z.N.A.® Soil DNA Kit (Omega Bio-tek, Norcross, GA, USA) according to the

manufacturer's instructions. DNA quality was assessed by 1% agarose gel electrophoresis, and DNA concentration and purity were determined using a NanoDrop 2000 spectrophotometer (Thermo Scientific, USA). Using the extracted DNA as template, the V3–V4 hypervariable region of the 16S rRNA gene was amplified by PCR using primers 338F (5′-ACTCCTACGGGAGGCAGCAG-3′) and 806R (5′-GGACTACHVGGGTWTCTAAT-3′) with barcode sequences.

The PCR reaction mixture (20 μL) contained 4 μL of 5× TransStart FastPfu buffer, 2 μL of 2.5 mM dNTPs, 0.8 μL of each primer (5 μM), 0.4 μL of TransStart FastPfu DNA polymerase, and 10 ng of template DNA. The amplification program was as follows: initial denaturation at 95°C for 3 minutes, followed by 27 cycles of 95°C for 30 seconds, 55°C for 30 seconds, and 72°C for 30 seconds, with a final extension at 72°C for 10 minutes, and hold at 4°C (PCR system: ABI GeneAmp® 9700). PCR products were recovered using 2% agarose gel electrophoresis and purified using a DNA Gel Recovery and Purification Kit (Yuhua, China). Purified products were quantified using a Qubit 4.0 fluorometer (Thermo Fisher Scientific, USA).

Libraries were constructed using the NEXTFLEX® Rapid DNA-Seq Kit, and sequencing was performed on the Illumina NextSeq 2000 platform.

2.3 Serum metabolomics analysis

For serum metabolomic profiling, 100 μL of serum was transferred to a 1.5-mL centrifuge tube, and 400 μL of extraction solution (acetonitrile:methanol = 1:1, v/v)

containing four internal standards, including L-2-chlorophenylalanine at 0.02 mg/mL, was added. The mixture was vortexed for 30 seconds, subjected to low-temperature ultrasonic extraction for 30 minutes at 5°C and 40 kHz, and then allowed to stand at −20°C for 30 minutes. Samples were centrifuged at 13,000 × g for 15 minutes at 4°C. The supernatant was transferred and evaporated to dryness under a gentle stream of nitrogen. The residue was reconstituted in 100 μL of reconstitution solution (acetonitrile:water = 1:1, v/v), vortexed, and subjected to low-temperature ultrasonic extraction for 5 minutes at 5°C and 40 kHz. After centrifugation at 13,000 × g for 10 minutes at 4°C, the supernatant was transferred to an autosampler vial with an insert for LC-MS analysis.

An UHPLC-Orbitrap Exploris 480 system was used for liquid chromatography–mass spectrometry (LC-MS) analysis. Chromatographic separation was performed on an HSS T3 column (100 mm × 2.1 mm, 1.8 μm) with mobile phase A consisting of 0.1% formic acid in water/acetonitrile (95:5, v/v) and mobile phase B consisting of 0.1% formic acid in acetonitrile/isopropanol/water (47.5:47.5:5, v/v/v). The flow rate was 0.40 mL/min, and the column temperature was maintained at 40°C. Mass spectrometry was performed in both positive and negative ion modes over a scan range of m/z 70–1050. The ion source temperature was set at 450°C, with spray voltages of 3500 V in positive mode and −3000 V in negative mode. Collision energies of 20, 40, and 60 V were applied cyclically.

2.4 Statistical analysis

All data are presented as the mean ± SEM. Statistical analyses were performed using SPSS 25.0. Comparisons between two groups were conducted using the independent-samples t-test for normally distributed data with equal variances or the Mann–Whitney U test for non-normally distributed data. $P < 0.05$ was considered statistically significant.

Microbiome data analysis: Alpha diversity indices (Chao1 and Shannon) were calculated using mothur, and intergroup differences were assessed using the Wilcoxon rank-sum test. Principal coordinate analysis (PCoA) based on Bray–Curtis distances was performed, and PERMANOVA was used to assess significant differences in community structure between groups. Species correlation network analysis was performed based on Spearman correlations ($|r| > 0.6$, $P < 0.05$). Metabolomics data processing: Principal component analysis (PCA) was performed using the R package ropls. Data quality was assessed using quality-control (QC) samples interspersed throughout the analytical run; the proportion of peaks with a relative standard deviation (RSD) below 30% increased from 73.2% before QC correction to 79.0% after correction. Differential metabolites were selected based on VIP > 1 and $P < 0.05$, and Benjamini–Hochberg false discovery rate (FDR) correction was applied. Metabolites with FDR < 0.05 were considered statistically robust, whereas those with $P < 0.05$ but FDR ≥ 0.05 are reported as trends. Finally, pathway annotation was performed using the KEGG database, and pathway enrichment analysis was conducted using Fisher's exact test.The datasets generated and analysed during the current study are available in the NCBI BioProject repository under accession number

PRJNA1544027, and in the MetaboLights repository under accession number MTBLS16044.

3 Results

3.1 Validation of the antibiotic exposure model

Fig. 1A showed the experimental feeding protocol for broilers. To confirm successful antibiotic administration, serum concentrations of the antibiotics and their metabolites were measured in 35-day-old broilers (Fig. 1B–D). Compared with the control group, the antibiotic-treated group exhibited a 161% increase in metronidazole concentration , a significant 94% increase in its primary metabolite, desmethylmisonidazole, and a 13% increase in its hydroxylated metabolite, metronidazole-OH ($P < 0.001$). These findings confirmed that antibiotic administration through drinking water successfully achieved systemic exposure.

3.2 Effects of antibiotic treatment on intestinal and organ development in broilers at different ages

Table 1 showed that changes in the organ indices of broilers at days 14, 21, and 35. On day 35, the thymus and spleen indices were 26% (P = 0.025) and 46% (P = 0.014) lower, respectively, in the antibiotic-treated group than in the control group. The bursa of Fabricius index decreased by 14%, although the difference was not significant ($P = 0.212$). These findings indicate that prolonged exposure to a broad-spectrum antibiotic cocktail suppressed immune development in broilers. The indices of the liver, heart, kidney, and pancreas were also reduced to varying degrees

in the antibiotic-treated group at different ages, with significant differences observed in some comparisons ($P < 0.05$) .The lengths of the duodenum, jejunum, ileum and colorectum were also significantly reduced by 14–21% in the antibiotic-treated group ($P < 0.05$). Collectively, these results demonstrate that antibiotic cocktail exposure induces systemic growth suppression in broilers, manifested by impaired immune and intestinal development.

3.3 Antibiotic treatment reshapes cecal microbial community structure

To determine the impact of antibiotic treatment on intestinal microbial ecology, cecal contents were subjected to 16S rRNA sequencing. Alpha diversity analysis revealed no significant difference in the Chao1 index between the two groups (Fig. 2A, P =0.1798); However, the Shannon index was significantly decreased, while the Simpson index was significantly increased in the antibiotic-treated group (Fig. 2B–C, $P < 0.05$), indicating that antibiotic treatment increased the dominance of dominant gut taxa and simplified the community structure. Rarefaction curves for the Sobs index approached saturation across all samples, confirming adequate sequencing depth (Fig. 2D). Beta diversity analysis based on Bray–Curtis distances and PCoA revealed significant separation between the control and antibiotic-treated groups (R^2 = 0.325, P = 0.001, Fig. 2E), confirming that antibiotic treatment induced an overall shift in microbial community structure. The UpSet plot showed that ASVs shared by the two groups accounted for only 14% of the total, whereas unique ASVs represented 56% and 57% of the antibiotic-treated and control groups, respectively (Fig. 2F),

indicating substantial remodeling of community composition at the ASV level following antibiotic treatment.

At the phylum level, the control group was dominated by Bacillota, whereas the antibiotic-treated group exhibited a significant increase in the relative abundance of Pseudomonadota, accompanied by a decrease in Bacillota (Fig. 2G). Statistical analysis confirmed a significant difference in Pseudomonadota abundance between the two groups ($P = 0.020$, Fig. 2H). At the genus level, we identified the top 10 genera showing significant differences in relative abundance. The control group was primarily characterized by *Lactobacillus* and *Ligilactobacillus*, both of which were significantly reduced following antibiotic treatment ($P < 0.01$), along with a significant reduction in *Litchfieldia* ($P < 0.05$). In contrast, the antibiotic-treated group showed significant enrichment of *Phascolarctobacterium*, *Escherichia-Shigella*, and *Enterococcus* ($P < 0.05$) (Fig. 2I–J). These results indicate that antibiotic treatment did not eliminate intestinal bacteria but instead selectively enriched a highly specialized, stress-tolerant microbial community dominated by opportunistic pathogens.

3.4 Antibiotic treatment affects gut microbial functional potential

We used LEfSe analysis to identify the top 10 species with the highest LDA scores in each group at the species level (Fig. 3A). The results showed that the control group was predominantly characterized by known beneficial species, whereas the antibiotic group was enriched in multiple opportunistic pathogens (LDA > 4),

indicating that antibiotic treatment disrupted gut microecological balance. Assessment using the Gut Microbiome Health Index (GMHI) further revealed that the antibiotic group had a significantly lower composite score than the control group ($P < 0.05$, Fig. 3B), indicating impaired gut ecosystem function.

To explore the functional changes underlying these compositional shifts, we performed functional prediction using PICRUSt2. Comparison of KEGG pathway abundances revealed that antibiotic treatment significantly downregulated carbohydrate metabolism, including glycolysis/gluconeogenesis and pyruvate metabolism; amino acid metabolism, such as glycine, serine, and threonine metabolism; nucleotide metabolism, including purine and pyrimidine metabolism; and protein synthesis-related pathways, including ribosome and aminoacyl-tRNA biosynthesis ($P < 0.05$). Conversely, pathways associated with ABC transporters and quorum sensing were significantly upregulated in the antibiotic group ($P < 0.05$) (Fig. 3C). These findings suggest that surviving bacteria reduced basal metabolic activity while shifting toward a survival strategy characterized by enhanced nutrient uptake and coordinated group behaviors to cope with stress.

To further investigate the ecological drivers underlying these functional changes, BugBase phenotype prediction was performed (Fig. 3D–E). The results showed that antibiotic treatment significantly increased the relative abundance of stress-tolerant, facultatively anaerobic, and potentially pathogenic phenotypes while decreasing the relative abundance of aerobic phenotypes ($P < 0.05$). These phenotypic shifts were

consistent with the depletion of beneficial genera, such as Lactobacillus, and the enrichment of opportunistic pathogens.

3.5 Antibiotic treatment depletes microbiota-derived metabolites

Fig. 4 presents the effects of antibiotic treatment on host serum metabolomic profiles. The PLS-DA score plot revealed clear separation between the control and antibiotic groups (Fig. 4A), while 200 permutation tests validated the robustness of the model (Fig. 4B), indicating that antibiotic exposure induced systemic metabolic alterations. Volcano plot analysis identified 341 differential metabolites (VIP > 1, $P <$ 0.05), including 98 upregulated and 243 downregulated metabolites (Fig. 4C). The number of downregulated metabolites was approximately 2.5 times that of upregulated metabolites, suggesting that antibiotic exposure primarily caused a systemic reduction in circulating metabolites.

Among the 341 differential metabolites, 20 representative metabolites were selected for in-depth analysis. The heatmap clearly separated the two groups based on these metabolites (Fig. 4D), while Figure 4E presents their fold changes, VIP values, and significance levels. Notably, aside from the significant increases in antibiotics and their metabolites, the most prominent changes were observed in tryptophan-derived indole metabolites. Compared with the control group, the antibiotic group exhibited reductions of 46–53% in 5-hydroxyindoxyl sulfate (FC = 0.47, VIP = 5.85, $P < 0.001$), quinoline 1-oxide (FC = 0.54, VIP = 5.68, $P < 0.001$), and 2,8-quinolinediol (FC =

297 0.55, VIP = 4.81, $P < 0.001$), providing direct evidence of a systemic collapse in gut
298 microbial tryptophan-to-indole metabolic capacity.

299 KEGG pathway enrichment analysis of all 341 differential metabolites identified
300 63 enriched pathways. Fig. 4F presents the top 20 pathways with $P < 0.05$, which
301 were mainly classified into four categories: Metabolism, Genetic Information
302 Processing, Cellular Processes, and Environmental Information Processing.
303 Comparison of these enriched pathways with PICRUSt2-predicted microbial
304 functional pathways revealed strong consistency in several core pathways, including
305 glycine, serine, and threonine metabolism; purine and pyrimidine metabolism;
306 aminoacyl-tRNA biosynthesis; and pyruvate metabolism. These findings strongly
307 support the hypothesis that antibiotics induce systemic host metabolic reprogramming
308 by reshaping gut microbial functions.

309 **3.6 Antibiotic treatment triggers systemic metabolic reprogramming in broilers**

310 We performed a correlation network analysis of 20 core metabolites based on
311 Spearman correlation coefficients ($|r| > 0.6$, $P < 0.05$). The results revealed distinct
312 clustering patterns among metabolites within the same functional category (Fig. 4G),
313 indicating multilayered metabolic reprogramming in response to the loss of
314 microbiota-derived metabolites.

315 **Energy metabolic reprogramming**

316 Antibiotic treatment induced significant alterations in energy metabolism,
317 characterized by a shift from glucose metabolism toward fatty acid and amino acid

oxidation. Fatty acid oxidation was enhanced, as evidenced by elevated levels of 3-hydroxybutyrylcarnitine (FC = 1.18, VIP = 2.76, $P < 0.05$) and O-acetylcarnitine (FC = 1.06, VIP = 1.95, $P < 0.05$). Glycolysis was activated, as indicated by increased pyruvate levels (FC = 1.05, VIP = 1.73, $P < 0.05$), whereas TCA cycle activity was impaired, as indicated by altered succinate levels (FC = 0.98, VIP = 1.00, $P < 0.05$). Concurrently, branched-chain amino acid catabolism increased, as evidenced by elevated levels of ketoleucine (FC = 1.03, VIP = 1.68, $P < 0.05$) and 3-methyl-2-oxovaleric acid (FC = 1.04, VIP = 1.80, $P < 0.05$). Overall, this pattern indicates that glycolysis was activated but accompanied by TCA cycle dysfunction, with compensatory increases in fatty acid and amino acid oxidation.

Amino acid metabolic disturbance

Multiple amino acids were depleted in the antibiotic group, including L-tyrosine (FC = 0.98, VIP = 1.25, $P = 0.037$) and L-cysteine (FC = 0.97, VIP = 1.43, $P = 0.011$). Concurrently, protein degradation was enhanced, as indicated by the accumulation of the dipeptides Val-Val (FC = 1.21, VIP = 2.56, $P = 0.008$) and Val-Leu (FC = 1.36, VIP = 3.36, $P = 0.007$).

Oxidative stress activation

Following antibiotic exposure, the endogenous antioxidant defense system was activated, as evidenced by increased concentrations of ascorbic acid (FC = 1.16, VIP = 2.72, $P = 0.014$) and ergothioneine (FC = 1.08, VIP = 2.16, $P = 9.85 \times 10^{-5}$). Meanwhile, the DNA oxidative damage marker 5-hydroxymethylcytosine (FC = 1.09,

VIP = 2.48, $P = 3.34 \times 10^{-6}$) was significantly elevated, indicating that oxidative stress had extended to the nucleic acid level.

Nucleotide metabolic suppression

De novo purine biosynthesis was inhibited, as reflected by reduced levels of AICAR (FC = 0.73, VIP = 2.94, $P = 0.023$), a key intermediate in de novo purine nucleotide biosynthesis. This significant reduction suggests impaired DNA/RNA synthesis and reduced cell proliferation capacity.

Phospholipid remodeling

The serum phospholipid profile was significantly altered, with reduced levels of LPC(18:1) (FC = 0.99, VIP = 1.07, $P = 0.00066$) and PC(14:0/0:0) (FC = 0.95, VIP = 2.02, $P = 7.60 \times 10^{-5}$), indicating systemic membrane remodeling. These changes suggest that antibiotic-induced metabolic reprogramming extended to cell membrane composition, potentially affecting membrane fluidity and signal transduction.

Correlation analysis between gut microbiota and serum metabolite alterations

Spearman correlation analysis was performed between core genera and representative metabolites (Fig. 5). The results showed that the antibiotic group's signature opportunistic pathogens, *Escherichia-Shigella* and *Enterococcus*, exhibited highly consistent correlation patterns. The abundances of both genera were significantly negatively correlated with tryptophan metabolites (5-hydroxyindoxyl sulfate, quinoline 1-oxide, and 2,8-quinolinediol) (*Escherichia-Shigella*: $r = -0.83$ to -0.82, $P < 0.001$; *Enterococcus*: $r = -0.75$ to -0.72, $P < 0.01$) and positively

correlated with the antibiotic metabolite metronidazole (r = 0.73 to 0.58, $P < 0.05$). Additionally, both genera showed positive correlation trends with the host fatty acid oxidation marker 3-hydroxybutyrylcarnitine (*Enterococcus*: r = 0.76, $P = 0.004$; *Escherichia-Shigella*: r = 0.43, $P > 0.05$), the DNA oxidative damage marker 5-hydroxymethylcytosine (*Enterococcus*: r = 0.77, $P = 0.003$; *Escherichia-Shigella*: r = 0.57, $P > 0.05$), and branched-chain amino acid catabolites (3-methyl-2-oxovaleric acid and ketoleucine).

In contrast, the control group's beneficial genera, *Lactobacillus* and *Ligilactobacillus*, showed significant positive correlations with 5-hydroxyindoxyl sulfate (*Lactobacillus*: r = 0.82, $P = 0.001$; *Ligilactobacillus*: r = 0.79, $P = 0.002$) and significant negative correlations with the antibiotic metabolite metronidazole (*Lactobacillus*: r = −0.66, $P = 0.020$; *Ligilactobacillus*: r = −0.79, $P = 0.002$), as well as with various energy- and stress-related metabolites, including pyruvic acid, O-acetylcarnitine, and ketoleucine.

These results indicate that antibiotic exposure reduced beneficial bacteria, including *Lactobacillus* and *Ligilactobacillus*, while promoting the expansion of opportunistic pathogens such as *Escherichia-Shigella* and *Enterococcus*. These concurrent microbial shifts collectively drove a systemic loss of tryptophan-to-indole metabolic function and may have contributed to host metabolic reprogramming by affecting energy metabolism and oxidative stress pathways.

4 Discussion

In this study, prolonged exposure to a broad-spectrum antibiotic cocktail significantly reduced immune organ indices (spleen, bursa of Fabricius, and thymus) in broilers, as well as the relative weights of parenchymal organs, including the heart and kidneys, and markedly shortened the small intestine and cecum. These findings demonstrate the systemic growth-suppressive effects of antibiotic exposure. Traditional explanations for these effects have largely focused on short-chain fatty acids (SCFAs)—fermentation products of the gut microbiota—as key molecules linking microbial activity to host immunity and barrier function [18,19]. However, our study revealed that antibiotic treatment profoundly suppressed the conversion of tryptophan into indole derivatives in the bloodstream. Specifically, the depletion of indole-producing core microbiota, particularly *Lactobacillus*, together with the expansion of opportunistic pathogens, such as *Enterobacteriaceae*, led to marked reductions in circulating indole metabolites, including 5-hydroxyindoxyl sulfate, quinoline 1-oxide, and 2,8-quinolinediol (Fig. 6). This ultimately triggered widespread metabolic adaptation and dysregulation in the host across energy, amino acid, nucleotide, and lipid metabolism, manifesting as impaired growth performance and organ development.

4.1 Antibiotic-induced gut microbial functional dysbiosis: a shift in microbial survival strategies

Our results demonstrate that long-term antibiotic treatment does not simply reduce the overall abundance of intestinal microbiota in broilers; rather, it impairs microbial fitness and ecological functions. Beneficial bacterial populations were

substantially depleted, whereas the relative abundances of opportunistic pathogens and potentially resistant taxa increased. At the phylum level, Pseudomonadota were significantly enriched, while at the genus level, *Enterobacteriaceae*-related taxa were markedly expanded. Similarly, clinical studies have reported that antibiotic treatment promotes the expansion of *Enterobacteriaceae* and other pathogens, such as *Enterococcus faecalis* and *Fusobacterium* nucleatum, accompanied by the depletion of *Bifidobacterium* and butyrate-producing bacteria [20]. However, other studies have found that antibiotic treatment simultaneously reduces disease-associated bacteria, including *Clostridium perfringens*, *Ruminococcus*, and *Klebsiella pneumoniae*, as well as beneficial species such as *Faecalibacterium prausnitzii*[21]. These discrepancies may be attributed to differences in antibiotic class, dosage, and treatment duration.

Functional gene prediction revealed downregulation of core metabolic pathways, including glycolysis, amino acid metabolism, nucleotide metabolism, and ribosome biosynthesis, indicating a global reduction in the metabolic output of the surviving community—highly consistent with the serum metabolomic profiles. Concurrently, the surviving community appeared to shift toward alternative survival strategies: predicted ABC transporter pathways were enriched, consistent with enhanced nutrient scavenging [22], while upregulation of quorum-sensing pathways promoted biofilm formation, virulence factor expression, and coordinated stress resistance [23]. These results indicate that antibiotic-selected microbial populations not only possess greater resistance potential but, more importantly, exhibit attenuated broad-spectrum

metabolic functions beneficial to the host while redirecting resources toward nutrient acquisition strategies that favor their own proliferation. This shift from "metabolic symbiosis" to "survival and defense" likely represents a key factor contributing to host metabolic substrate deficiency and growth suppression.

4.2 Microbiota-derived tryptophan metabolites: the critical link between dysbiosis and host metabolic reprogramming

The most notable finding of this study was the systemic depletion of tryptophan-derived indole metabolites in the antibiotic-treated group. Three indole metabolites—5-hydroxyindoxyl sulfate, quinoline 1-oxide, and 2,8-quinolinediol—were significantly reduced. Because these indole derivatives are predominantly generated by intestinal bacteria, their coordinated decline is consistent with a disruption of microbial tryptophan metabolism [24].

Indole metabolites serve as key ligands for the aryl hydrocarbon receptor (AhR), which plays a central role in regulating intestinal barrier integrity and immune homeostasis [25]. Studies have demonstrated that increasing colonic levels of AhR ligands, such as indole-3-aldehyde (IAld) and indole-3-acetic acid (IAA), can alleviate ulcerative colitis[26]. Conversely, impaired AhR signaling has been closely associated with increased intestinal permeability, systemic inflammation, and metabolic disorders [25,27,28]. The approximately 50% reduction in circulating indole metabolites observed here would be expected to reduce AhR ligand availability and may therefore compromise AhR signaling. Should it be confirmed, it could help explain the impaired intestinal development and the systemic metabolic disturbances

observed in this study.

4.3 Host metabolic reprogramming: an imbalance between damage and compensation

Metabolomic data revealed systemic metabolic remodeling in antibiotic-treated broilers, characterized by a dual pattern of "damage" and "compensation." On the damage side, first, the significant reduction in succinic acid, a TCA cycle intermediate, suggests that pyruvate generated through enhanced glycolysis failed to enter mitochondrial oxidative metabolism efficiently, indicating impaired mitochondrial function. Second, multiple amino acids, including tyrosine and cysteine showed global depletion. This not only indicates an insufficient supply of substrates for protein synthesis but also suggests that gut dysbiosis may affect host neurological function through the gut–brain axis, as tyrosine is a precursor of catecholamine neurotransmitters and tryptophan is a precursor of serotonin [29]. Extensive literature supports a close association between gut microbial dysbiosis, abnormalities in neurotransmitter metabolism, and behavioral changes [30,31]. Furthermore, reduced AICAR levels reflected impaired purine synthesis, potentially limiting cell proliferation and tissue repair, whereas elevated 5-hydroxymethylcytosine (5-hmC) levels indicated DNA oxidative damage, likely associated with reactive oxygen species accumulation and an increased burden on the antioxidant system [32].

Simultaneously, the host activated multiple compensatory mechanisms: elevated 3-hydroxybutyrylcarnitine indicated enhanced fatty acid β-oxidation as an alternative energy source to compensate for insufficient ATP production by the TCA cycle;

increased levels of the dipeptides Val-Val and Val-Leu suggested mobilization of endogenous skeletal muscle proteins, releasing branched-chain amino acids for energy supply; and elevated ascorbic acid (vitamin C) and ergothioneine indicated activation of the endogenous antioxidant defense system in response to oxidative stress. This compensatory pattern is consistent with findings from mammalian studies, in which antibiotic treatment has been shown to affect multiple metabolic pathways, including amino acid, lipid, and carbohydrate metabolism[33]. In a mouse model of atherosclerosis, antibiotic treatment similarly reduced tryptophan metabolism and disrupted lipid metabolism, changes closely associated with exacerbated lesion severity [34].

However, our metabolomic data suggest that this compensatory mode is insufficient to restore core anabolic pathways. Although energy supply was partially maintained, growth performance and organ development remained significantly impaired, indicating that the host had entered a state characterized by both "compensatory consumption" and "anabolic blockade." These findings suggest that, under conditions of gut microecological imbalance, the host attempts to meet basal energy requirements by enhancing fatty acid oxidation and mobilizing endogenous protein reserves, but this stress adaptation comes at the cost of growth and overall health.

5 Conclusions

This study demonstrates that prolonged exposure to a broad-spectrum antibiotic cocktail is accompanied by systemic metabolic reprogramming in broilers through a

"microbial disruption–metabolic compensation" mechanism. Antibiotic treatment caused gut dysbiosis, characterized by the depletion of indole-producing commensals and the expansion of opportunistic pathogens, together with systemic reductions in microbiota-derived tryptophan metabolites. This disruption was accompanied by widespread metabolic disturbances and ultimately impaired organ and intestinal development. Our findings highlight a central role for gut microbial tryptophan metabolism in maintaining host metabolic homeostasis and suggest that preserving this metabolic function may represent a potential therapeutic target for mitigating antibiotic-induced metabolic impairment.

Abbreviations

5-hmC	5-Hydroxymethylcytosine
ABC	ATP-Binding Cassette Transporters
AGP	Antibiotic growth promoters
AhR	Aryl hydrocarbon receptor
AICAR	5-Amino-1-(5-phospho-D-ribosyl)imidazole-4-carboxylic acid
FC	Fold Change
IAA	Indole-3-acetic acid
GMHI	Gut Microbiome Health Index
LDA	Linear Discriminant Analysis
LPC	Lysophosphatidylcholine
PCoA	Principal Coordinate Analysis

PLS-DA Partial Least Squares Discriminant Analysis

TCA Tricarboxylic Acid Cycle

VIP Variable importance in projection

Authors' contributions

Juanjuan Xiong : Conceptualization, Methodology, Supervision,Writing – original draft. **Baofeng Chen :** Data Curation. **Hui Wang :** Visualization, Investigation. **Xinjie Bai:** Writing - Review & Editing.

Declaration of competing interests

The authors declare that they have no competing financial or personal interests that could have influenced the work reported in this paper. No professional or personal relationships with any product, service, or company could be construed as affecting the content or conclusions of this study.

Acknowledgements

We thank Shanghai Majorbio Bio-pharm Technology Co., Ltd. for technical support in metabolomics and 16S rRNA sequencing. We also acknowledge the Home for Researchers editorial team (www.home-for-researchers.com) for their assistance in figure preparation.

Funding

No

Data availability

The datasets generated and analysed during the current study are available in the NCBI BioProject repository under accession number PRJNA1544027, and in the MetaboLights repository under accession number MTBLS16044.

Ethics declaration

All animal experiments were approved by the Laboratory Animal Welfare and Ethics Committee of Jinling Institute of Technology and conducted in strict compliance with institutional and international animal welfare guidelines.

Consent for publication

No applicable

References

[1] Barrero MAO, Varón-López M, Peñuela-Sierra LM. Competing microorganisms with exclusion effects against multidrug-resistant Salmonella Infantis in chicken litter supplemented with growth-promoting antimicrobials. Vet World. 2025;18:1127-36.

[2] Plata G, Baxter NT, Susanti D, Volland-Munson A, Gangaiah D, Nagireddy A, et

557 al. Growth promotion and antibiotic induced metabolic shifts in the chicken gut
558 microbiome. Commun Biol. 2022;5:293.
559 [3] Uehara A, Maekawa M, Nakagawa K. Enhanced intestinal barrier function as the
560 mechanism of antibiotic growth promoters in feed additives. Biosci Biotechnol
561 Biochem. 2023;87:1381-92.
562 [4] Maria Cardinal K, Kipper M, Andretta I, Machado Leal Ribeiro A. Withdrawal of
563 antibiotic growth promoters from broiler diets: performance indexes and
564 economic impact. Poult Sci. 2019;98:6659-67.
565 [5] Xu Y, Xiao Y, Ai C, Huang Y, Zhou H, Li J, et al. Antibiotic growth promoters and
566 waxy corn enhance broiler growth performance through starch digestibility and
567 microbiota modulation in the crop and ileum. Poult Sci. 2025;104:105288.
568 [6] Han X, Qin Y, Guo J, Huang W, You Y, Zhan J, et al. IgA dysfunction induced by
569 early-lifetime low-dose antibiotics exposure aggravates diet-induced metabolic
570 syndrome. Antibiotics (Basel). 2025;14.
571 [7] Hou L, Cao S, Qiu Y, Xiong Y, Xiao H, Wen X, et al. Effects of early
572 sub-therapeutic antibiotic administration on body tissue deposition, gut
573 microbiota and metabolite profiles of weaned piglets. J Sci Food Agric.
574 2022;102:5913-24.
575 [8] He M, Shi J, Liu A, Xu YJ, Liu Y. Antibiotic-induced gut microbiota dysbiosis
576 altered host metabolism. Mol Omics. 2023;19:330-9.
577 [9] Thompson NT, Kitzenberg DA, Kao DJ. Persister-mediated emergence of
578 antimicrobial resistance in agriculture due to antibiotic growth promoters. AIMS

Microbiol. 2023;9:738-56.

[10] Agus A, Clément K, Sokol H. Gut microbiota-derived metabolites as central regulators in metabolic disorders. Gut. 2021;70:1174-82.

[11] Lin X, He K, Gu Z, Zhao X. Emerging chemophysiological diversity of gut microbiota metabolites. Trends Pharmacol Sci. 2024;45:824-38.

[12] Fishbein SRS, Mahmud B, Dantas G. Antibiotic perturbations to the gut microbiome. Nat Rev Microbiol. 2023;21:772-88.

[13] Mann ER, Lam YK, Uhlig HH. Short-chain fatty acids: linking diet, the microbiome and immunity. Nat Rev Immunol. 2024;24:577-95.

[14] Zeng SY, Liu YF, Zeng ZL, Zhao ZB, Yan XL, et al. Antibiotic-induced gut microbiota disruption promotes vascular calcification by reducing short-chain fatty acid acetate. Mol Med. 2024;30:130.

[15] Guo Q, He Y,Cao T, Lin C,Deng M, Cai H. Tryptophan-kynurenine metabolism: A link between the gut microbiota dysbiosis and cognitive impairment. Microbiol Res. 2026;307:128481.

[16] Hu J, Chen J, Xu X, Hou Q, Ren J, Yan X. Gut microbiota-derived 3-phenylpropionic acid promotes intestinal epithelial barrier function via AhR signaling. Microbiome. 2023;11:102.

[17] Shi D, Cui Y, Liang H, Wei Q, Huang J, Cao J. Gut microbiota-derived tryptophan metabolite indole-3-carboxaldehyde enhances intestinal barrier function via aryl hydrocarbon receptor/AMP-activated protein kinase signaling activation. Anim Biosci. 2026;39:250225.

[18] Ottria R, Mirmajidi S, Ciuffreda P. Gut microbiota-derived short-chain fatty acids in inflammatory bowel disease: Mechanistic insights into gut inflammation, barrier function, and therapeutic potential. Int J Mol Sci. 2026;27.

[19] Yu J, Li W, Xu Y, Tang J. Gut microbiota-derived short-chain fatty acids (SCFAs): immunomodulatory effects and therapeutic potential in infections. Clin Microbiol Rev. 2026;e0036825.

[20] Mikkelsen KH, Forslund SK, Allin KH, Nielsen T, Feng Q, Zhang C, et al. Recovery of gut microbiota of healthy adults following antibiotic exposure. Nat Microbiol. 2018;3:1255-65.

[21] Dubinsky V, Reshef L, Bar N, Keizer D, Golan N, Rabinowitz K, et al. Predominantly antibiotic-resistant intestinal microbiome persists in patients with pouchitis who respond to antibiotic therapy. Gastroenterology. 2020;158:610-24.e613.

[22] Andersen V, Svenningsen K, Knudsen LA, Hansen AK, Holmskov U, Stensballe A, et al. Novel understanding of ABC transporters ABCB1/MDR/P-glycoprotein, ABCC2/MRP2, and ABCG2/BCRP in colorectal pathophysiology. World J Gastroenterol. 2015;21:11862-76.

[23] Núño K, Jensen AS, O'Connor G, Houston TJ, Dikici E, Zingg JM, et al. Insights into women's health: Exploring the vaginal microbiome, quorum sensing dynamics, and therapeutic potential of quorum sensing quenchers. Mol Aspects Med. 2024;100:101304.

[24] Zhao P, Chen Y, Zhou S, Li F. Microbial modulation of tryptophan metabolism

links gut microbiota to disease and its treatment. Pharmacol Res. 2025;219:107896.

[25] Liu M,, Li S, Zhu X, Wang Z, Sun H, Liu B. Tryptophan metabolism mediated by the gut microbiota inhibits pyroptosis via the AhR signaling pathway to maintain intestinal epithelial homeostasis. Microbiome. 2026;14.

[26] Zhang D, Wu J, Feng H, Tang P, Zhou Y, Zhao C, et al. Gastrodin ameliorates ulcerative colitis via modulating gut microbial tryptophan metabolism and AhR/NLRP3 pathway. Phytomedicine. 2025;147:157217.

[27] Rothhammer V, Kenison JE, Mayo L, Chao CC, Patel B, Yan R, et al. Type I interferons and microbial metabolites of tryptophan modulate astrocyte activity and central nervous system inflammation via the aryl hydrocarbon receptor. Nat Med. 2016;22:586-97.

[28] Jing W, Dong S, Xu Y, Liu J, Ren J, Liu X, et al. Gut microbiota-derived tryptophan metabolites regulated by Wuji Wan to attenuate colitis through AhR signaling activation. Acta Pharm Sin B. 2025;15:205-23.

[29] Hendel M, Gut-Misiaga M, Gil A, Kwiendacz H, Tan BYQ, Fothergill JL, et al. Gut microbiota and stroke: New insights into the gut-brain-vascular axis. Curr Atheroscler Rep. 2026;28:18.

[30] Cryan JF, O'Riordan KJ, Cowan CSM, Sandhu KV, Bastiaanssen TFS, Boehme M, et al. The microbiota-gut-brain axis. Physiol Rev. 2019;99:1877-2013.

[31] Ni Y, Tong Q, Xu M, Gu J, Ye H. Gut microbiota-induced modulation of the central nervous system function in Parkinson's disease through the gut-brain axis

and short-chain fatty acids. Mol Neurobiol. 2025;62:2480-92.

[32] Zheng K, Lyu Z, Chen J, Chen G. 5-Hydroxymethylcytosine: Far beyond the intermediate of DNA demethylation. Int J Mol Sci. 2024;25.

[33] Lei H, Shuting C, Yueqin Q. Effects of early sub-therapeutic antibiotic administration and its subsequent withdrawal on body composition, gut microbiota and metabolite profiles in a pig model. Research Square. 2021.

[34] Kappel BA, De Angelis L, Heiser M, Ballanti M, Artati A, Paoluzi OA, et al. Cross-omics analysis revealed gut microbiome-related metabolic pathways underlying atherosclerosis development after antibiotics treatment. Mol Metab. 2020;36:100976.

Figure legends

Fig. 1. Experimental design and antibiotic exposure verification

(A). Schematic diagram of the animal experimental design. (B). Metronidazole. (C). Desmethylmisonidazole. (D). Metronidazole-OH. Data are presented as mean ± SEM. ***P < 0.001 compared with the Control group (Student's t-test).

Fig. 2. Antibiotic-induced alterations in cecal microbial community structure

(A). Chao richness index. (B). Shannon diversity index. (C). Simpson diversity index. (D). Rarefaction curves of Sobs index. (E). Principal coordinate analysis (PCoA) based on Bray-Curtis distances at the ASV level. (F). UpSet plot showing shared and unique ASVs across groups. (G). Phylum-level relative abundance. (H). Phylum-level differential abundance. (I). Genus-level relative abundance. (J). Genus-level

667 differential abundance analysis.

668 Fig. 3. Gut microbial functional potential and phenotypic traits predicted by

669 PICRUSt2 and BugBase.

670 (A). LEfSe analysis showing the top 10 species with the highest LDA scores in each

671 group. (B). Gut Microbiome Health Index (GMHI) comparison between groups. (C).

672 PICRUSt2-predicted functional pathways at KEGG Level 3 classification. (D-E).

673 BugBase phenotype prediction showing the relative abundance of nine phenotypic

674 traits.

675 Fig. 4. Serum metabolomic profiling and identification of core differential metabolites

676 (A). PLS-DA score plot showing global metabolomic separation between Control and

677 Antibiotic groups. (B). PLS-DA permutation test (200 iterations). (C). Volcano plot of

678 differential metabolites between Antibiotic and Control groups. (D). Heatmap of 20

679 representative core metabolites. (E). Bar plot showing fold change and VIP values of

680 the 20 core metabolites. (F). KEGG pathway enrichment analysis of all significant

681 differential metabolites. (G). Correlation network of the 20 core metabolites.

682 Fig. 5. Integrated correlation analysis between gut microbiota and host metabolites

683 Spearman correlation heatmap between core bacterial genera and core metabolites.

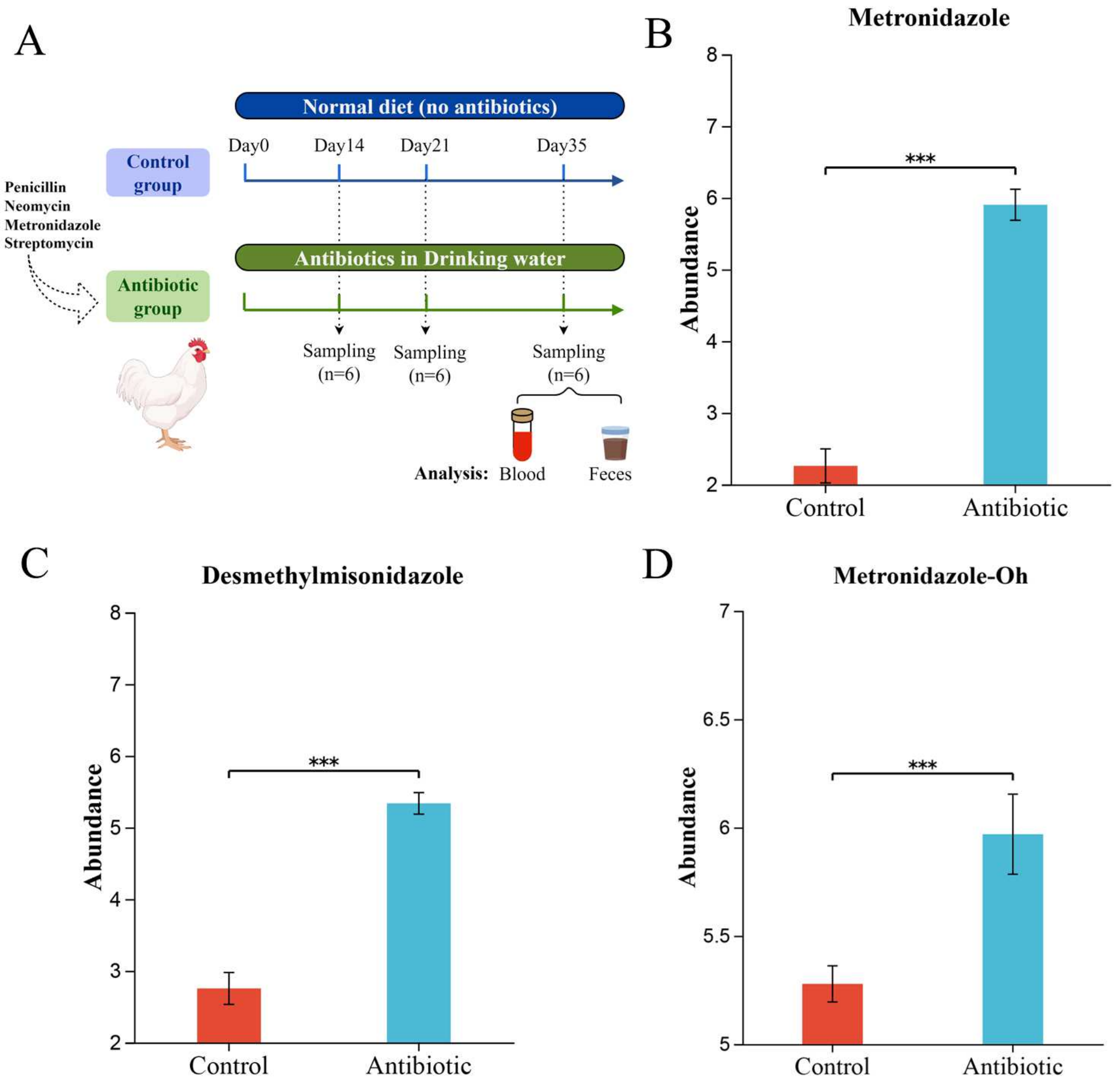
684 Rows represent bacterial genera (n = 15), columns represent representative

685 metabolites (n = 20). Color intensity indicates correlation coefficient (red: positive

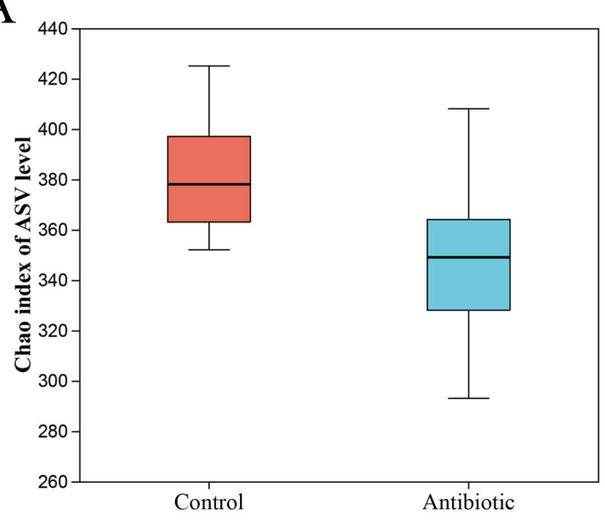
686 correlation; blue: negative correlation). *$P < 0.05$, **$P < 0.01$, ***$P < 0.001$.

687 Fig. 6. Schematic model of antibiotic-induced systemic metabolic reprogramming in

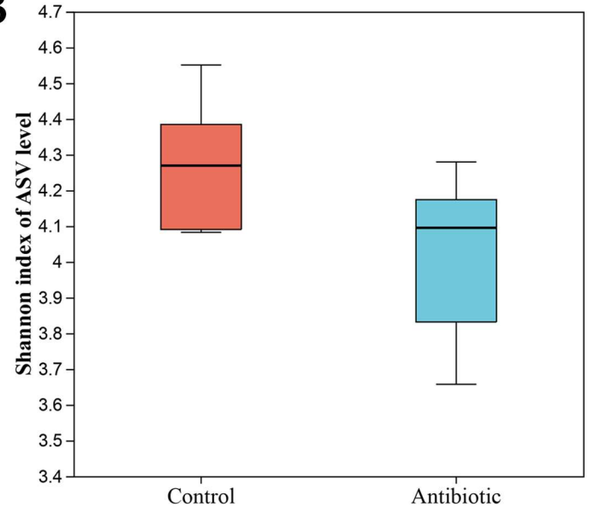
688 broilers


A
Normal diet (no antibiotics)
Day0
Day14
Day21
Day35
Control group
Penicillin
Neomycin
Metronidazole
Streptomycin
Antibiotic group
Antibiotics in Drinking water
Sampling (n=6)
Sampling (n=6)
Sampling (n=6)
Analysis: Blood
Feces
B
Metronidazole
Abundance
***
Control
Antibiotic
C
Desmethylmisonidazole
Abundance
***
Control
Antibiotic
D
Metronidazole-Oh
Abundance
***
Control
Antibiotic

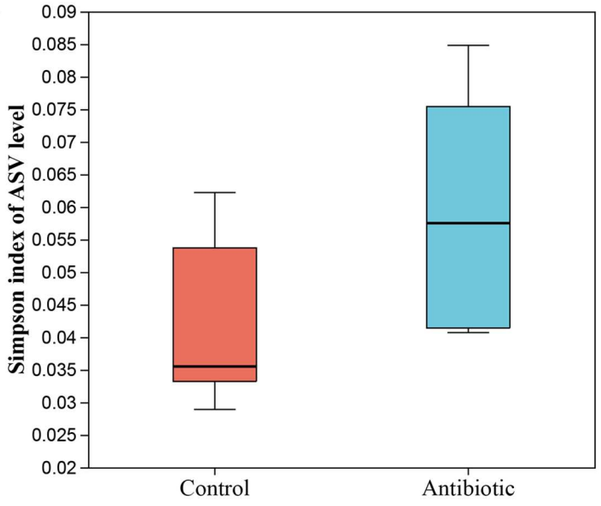
A


Chao index of ASV level
Control
Antibiotic

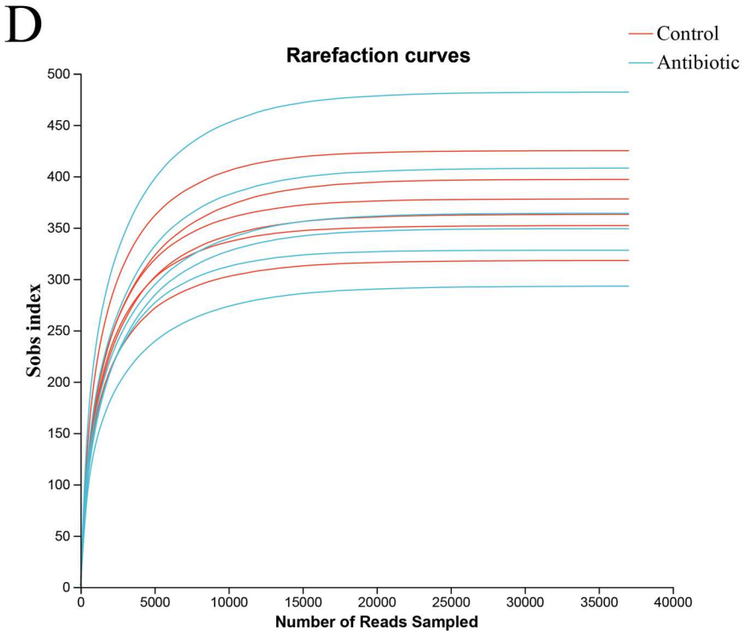
B


Shannon index of ASV level
Control
Antibiotic

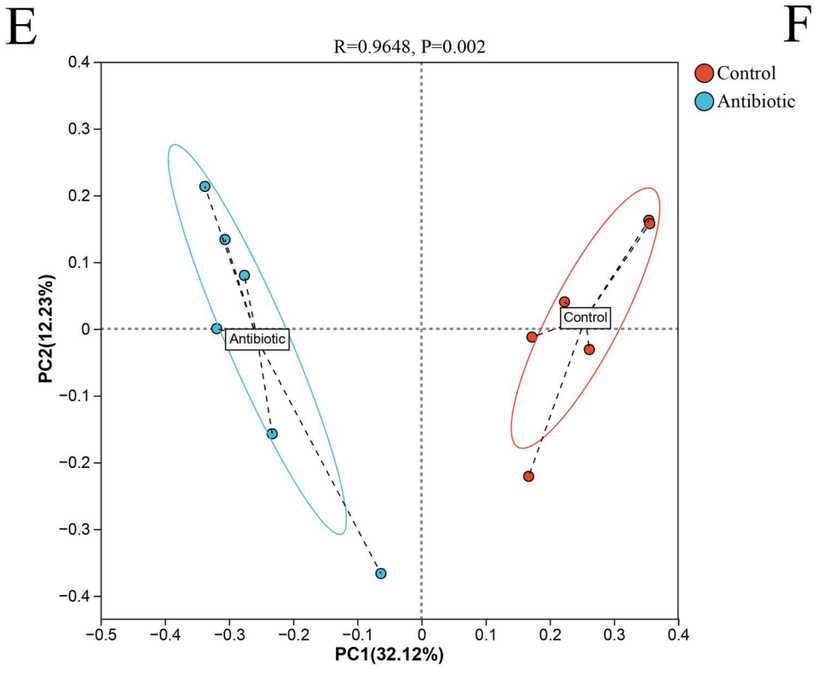
C


Simpson index of ASV level
Control
Antibiotic

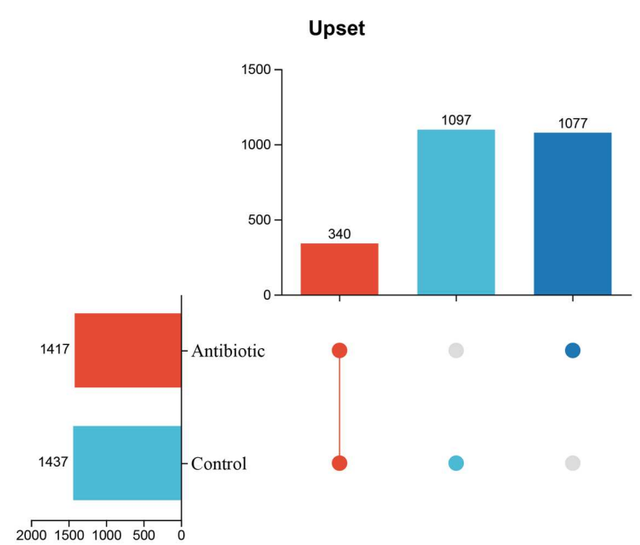
D


Rarefaction curves
Control
Antibiotic
Sobs index
Number of Reads Sampled

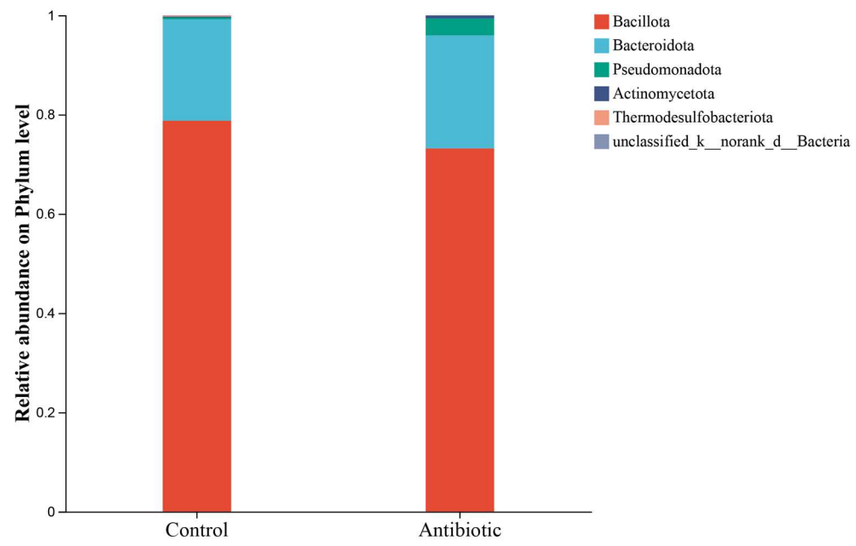
E


R=0.9648, P=0.002
Control
Antibiotic
PC2(12.23%)
PC1(32.12%)

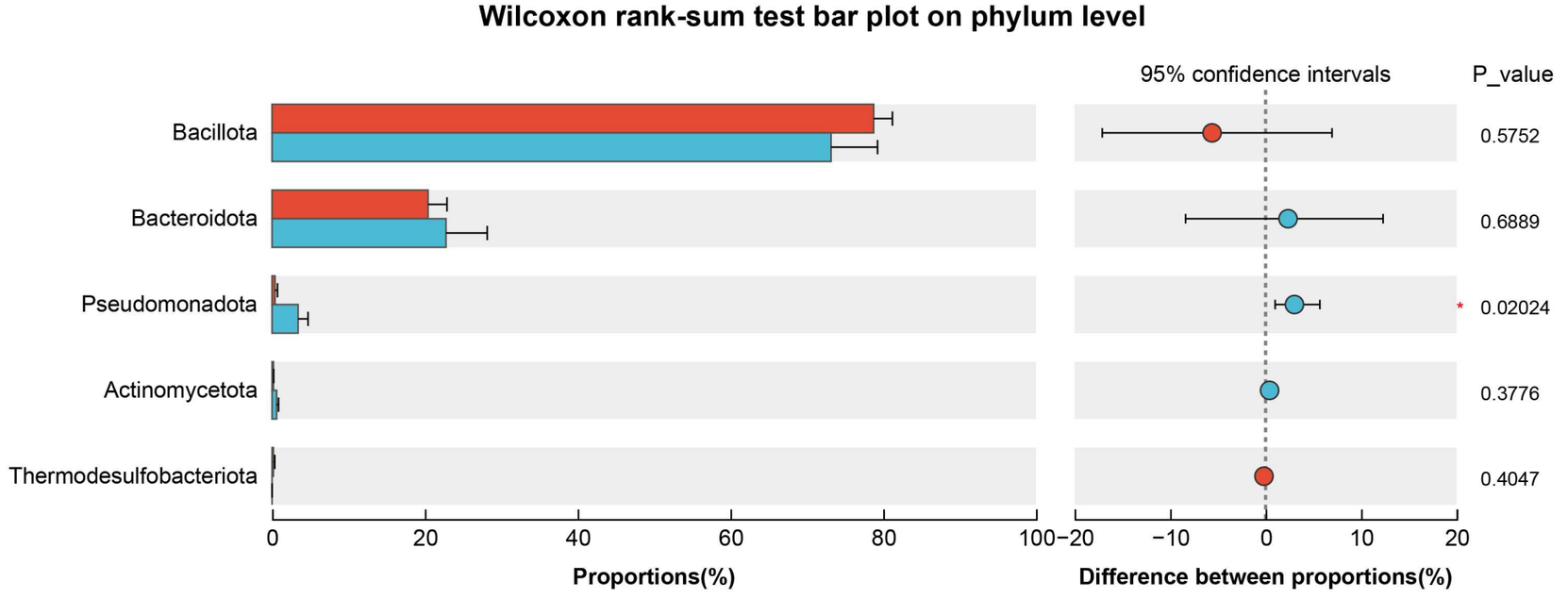
F


Upset
1500
1000
500
0
1097
1077
340
1417
1437
Antibiotic
Control
2000 1500 1000 500 0

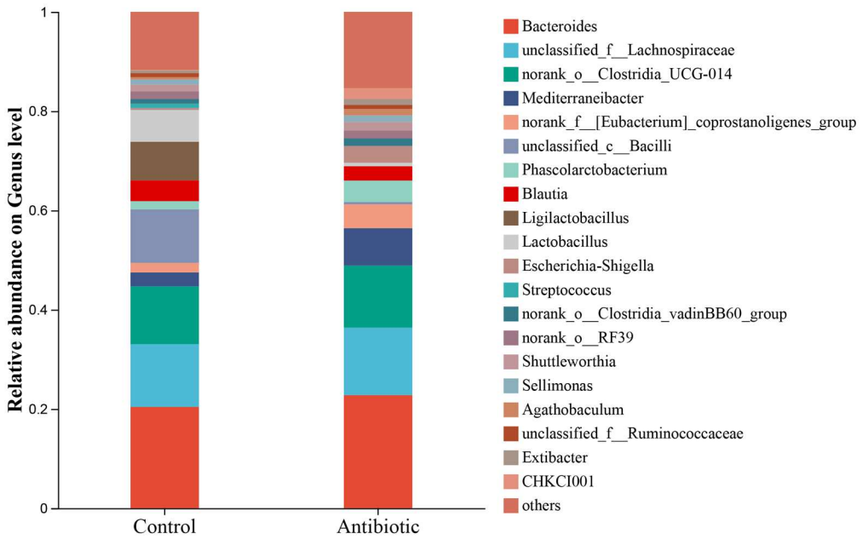
G


Relative abundance on Phylum level
Bacillota
Bacteroidota
Pseudomonadota
Actinomycetota
Thermodesulfobacteriota
unclassified_k__norank_d__Bacteria
Control
Antibiotic

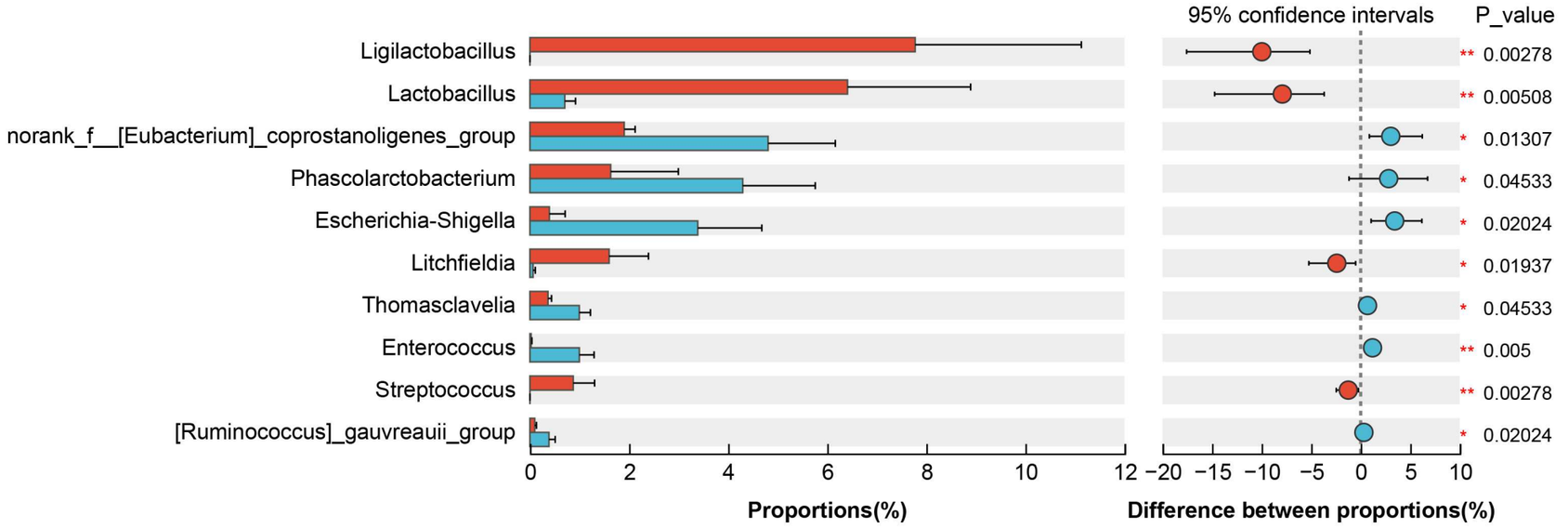
H

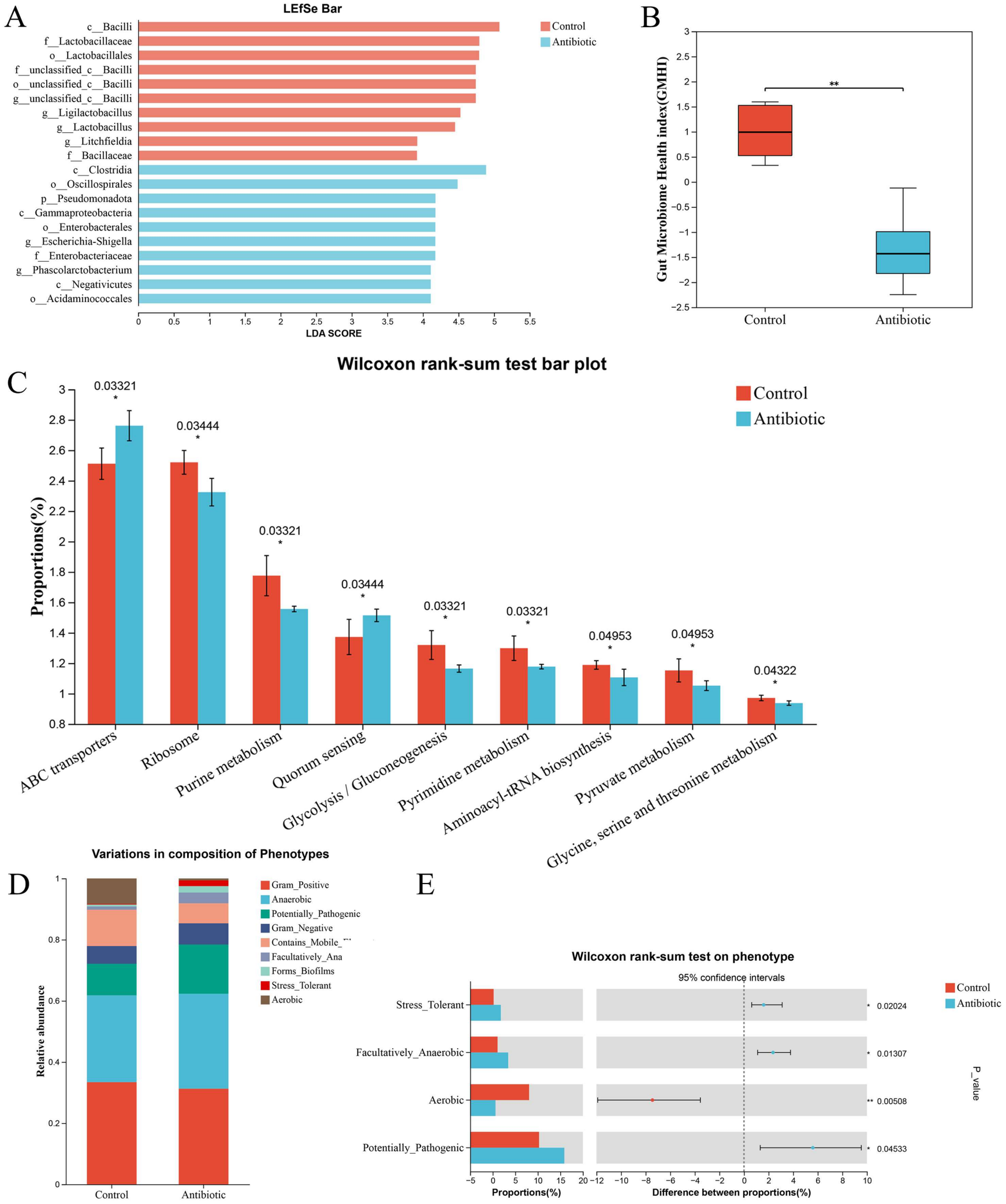

Wilcoxon rank-sum test bar plot on phylum level
95% confidence intervals
P_value
Bacillota
Bacteroidota
Pseudomonadota
Actinomycetota
Thermodesulfobacteriota
0.5752
0.6889
* 0.02024
0.3776
0.4047
Proportions(%)
Difference between proportions(%)

I

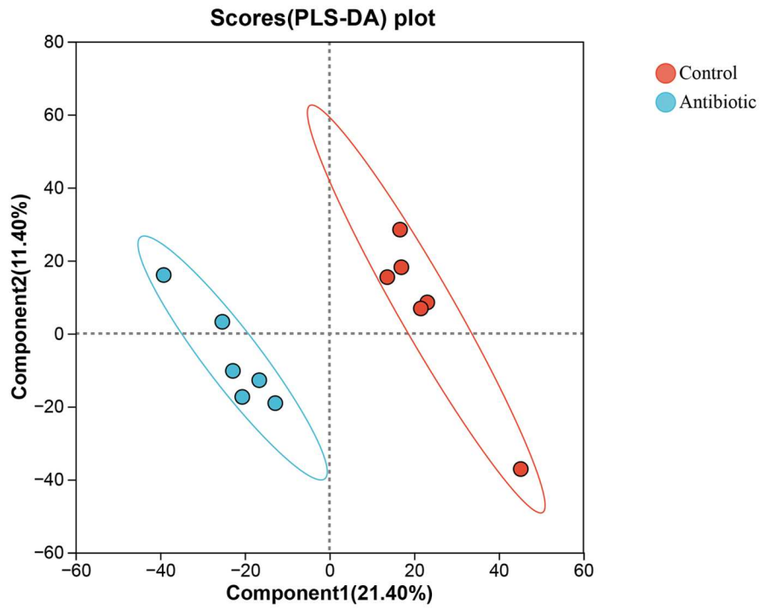

Relative abundance on Genus level
Bacteroides
unclassified_f__Lachnospiraceae
norank_o__Clostridia_UCG-014
Mediterraneibacter
norank_f__[Eubacterium]_coprostanoligenes_group
unclassified_c__Bacilli
Phascolarctobacterium
Blautia
Ligilactobacillus
Lactobacillus
Escherichia-Shigella
Streptococcus
norank_o__Clostridia_vadinBB60_group
norank_o__RF39
Shuttleworthia
Sellimonas
Agathobaculum
unclassified_f__Ruminococcaceae
Extibacter
CHKCI001
others
Control
Antibiotic

J

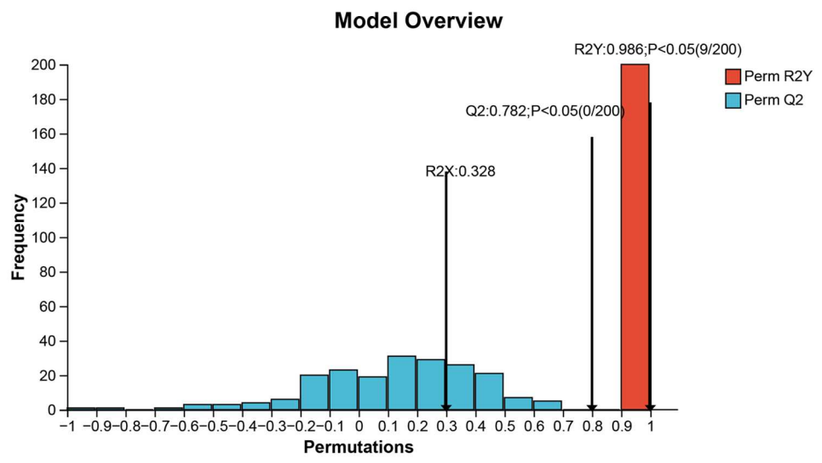

Wilcoxon rank-sum test bar plot on genus level
95% confidence intervals
P_value
Ligilactobacillus
Lactobacillus
norank_f__[Eubacterium]_coprostanoligenes_group
Phascolarctobacterium
Escherichia-Shigella
Litchfieldia
Thomasclavelia
Enterococcus
Streptococcus
[Ruminococcus]_gauvreauii_group
** 0.00278
** 0.00508
* 0.01307
* 0.04533
* 0.02024
* 0.01937
* 0.04533
** 0.005
** 0.00278
* 0.02024
Proportions(%)
Difference between proportions(%)


A
LEfSe Bar
c__Bacilli
f__Lactobacillaceae
o__Lactobacillales
f__unclassified_c__Bacilli
o__unclassified_c__Bacilli
g__unclassified_c__Bacilli
g__Ligilactobacillus
g__Lactobacillus
g__Litchfieldia
f__Bacillaceae
c__Clostridia
o__Oscillospirales
p__Pseudomonadota
c__Gammaproteobacteria
o__Enterobacterales
g__Escherichia-Shigella
f__Enterobacteriaceae
g__Phascolarctobacterium
c__Negativicutes
o__Acidaminococcales
Control
Antibiotic
LDA SCORE
B
Gut Microbiome Health index(GMHI)
**
Control
Antibiotic
C
Wilcoxon rank-sum test bar plot
Proportions(%)
0.03321
0.03444
0.03321
0.03444
0.03321
0.03321
0.04953
0.04953
0.04322
ABC transporters
Ribosome
Purine metabolism
Quorum sensing
Glycolysis / Gluconeogenesis
Pyrimidine metabolism
Aminoacyl-tRNA biosynthesis
Pyruvate metabolism
Glycine, serine and threonine metabolism
Control
Antibiotic
D
Variations in composition of Phenotypes
Relative abundance
Gram_Positive
Anaerobic
Potentially_Pathogenic
Gram_Negative
Contains_Mobile_
Facultatively_Ana
Forms_Biofilms
Stress_Tolerant
Aerobic
Control
Antibiotic
E
Wilcoxon rank-sum test on phenotype
95% confidence intervals
Stress_Tolerant
Facultatively_Anaerobic
Aerobic
Potentially_Pathogenic
0.02024
0.01307
0.00508
0.04533
P_value
Proportions(%)
Difference between proportions(%)
Control
Antibiotic

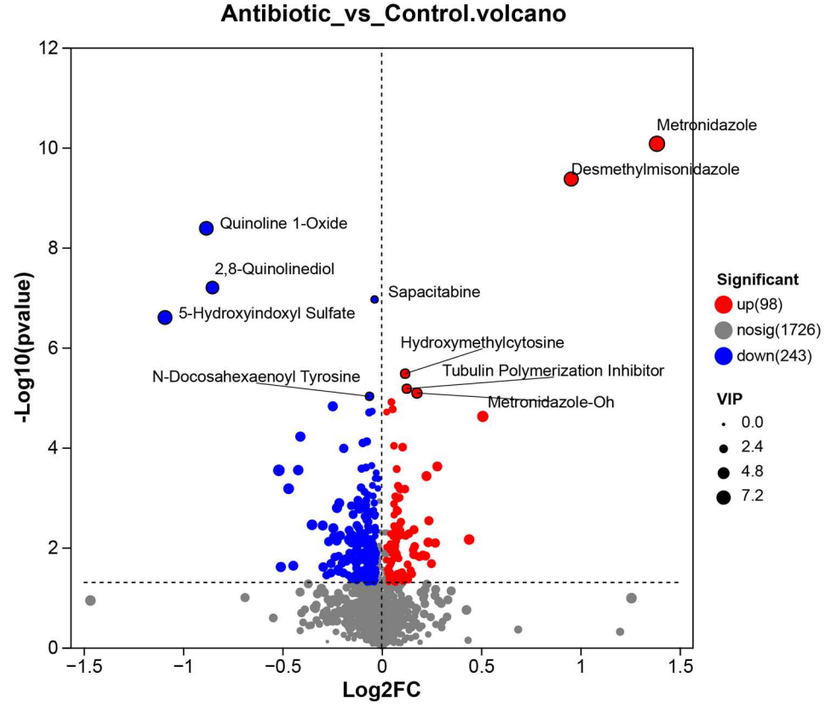
A


Scores(PLS-DA) plot
Control
Antibiotic
Component2(11.40%)
Component1(21.40%)

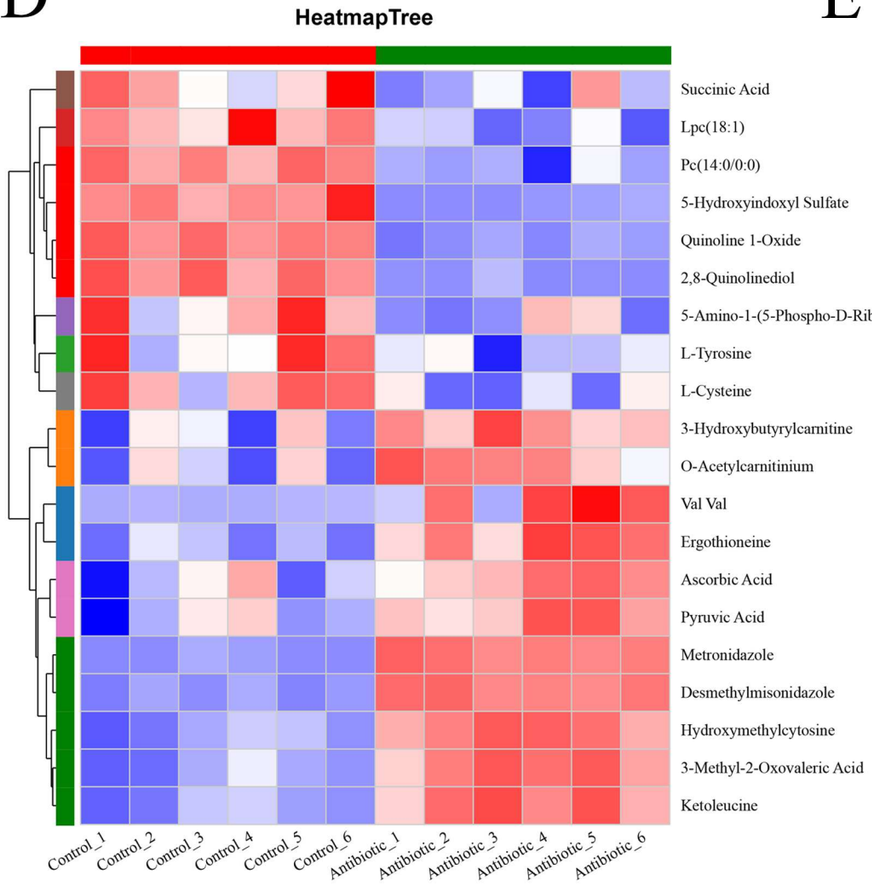
B


Model Overview
R2Y:0.986;P<0.05(9/200)
Q2:0.782;P<0.05(0/200)
R2X:0.328
Perm R2Y
Perm Q2
Frequency
Permutations

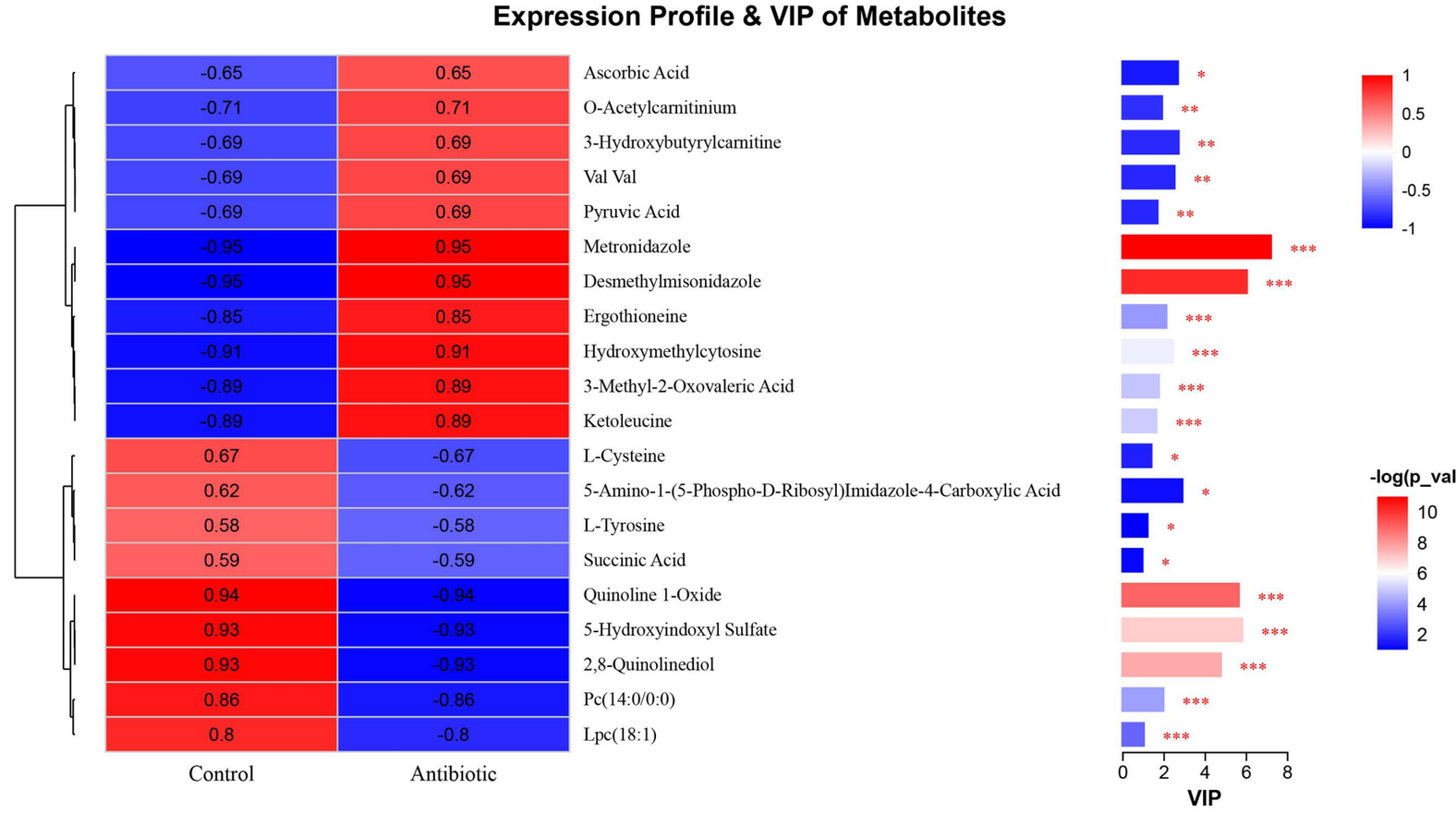
C


Antibiotic_vs_Control.volcano
Metronidazole
Desmethylmisonidazole
Quinoline 1-Oxide
2,8-Quinolinediol
Sapacitabine
5-Hydroxyindoxyl Sulfate
Hydroxymethylcytosine
Tubulin Polymerization Inhibitor
N-Docosahexaenoyl Tyrosine
Metronidazole-Oh
-Log10(pvalue)
Log2FC
Significant
up(98)
nosig(1726)
down(243)
VIP
0.0
2.4
4.8
7.2

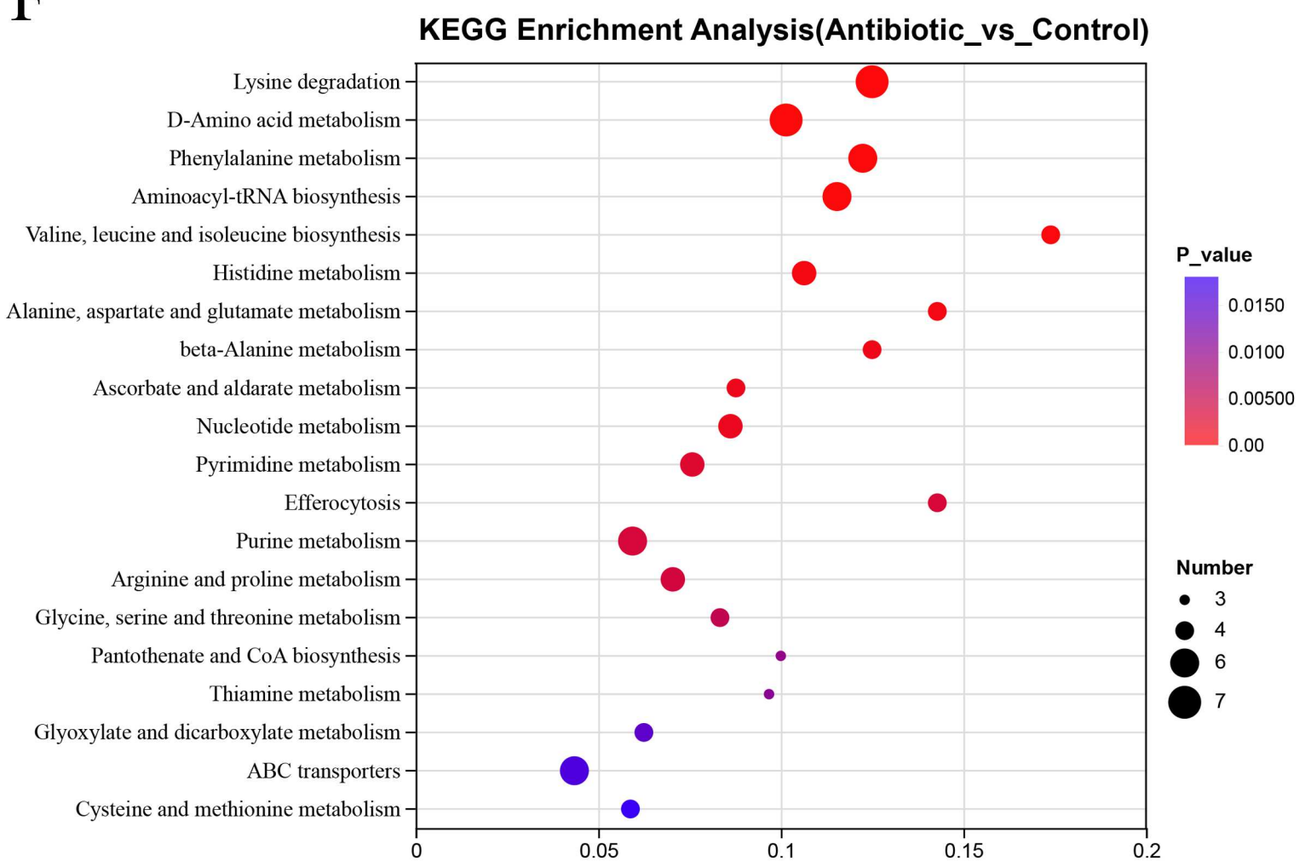
D


HeatmapTree
Succinic Acid
Lpc(18:1)
Pc(14:0/0:0)
5-Hydroxyindoxyl Sulfate
Quinoline 1-Oxide
2,8-Quinolinediol
5-Amino-1-(5-Phospho-D-Ribosyl)I...
L-Tyrosine
L-Cysteine
3-Hydroxybutyrylcarnitine
O-Acetylcarnitinium
Val Val
Ergothioneine
Ascorbic Acid
Pyruvic Acid
Metronidazole
Desmethylmisonidazole
Hydroxymethylcytosine
3-Methyl-2-Oxovaleric Acid
Ketoleucine
Control_1
Control_2
Control_3
Control_4
Control_5
Control_6
Antibiotic_1
Antibiotic_2
Antibiotic_3
Antibiotic_4
Antibiotic_5
Antibiotic_6

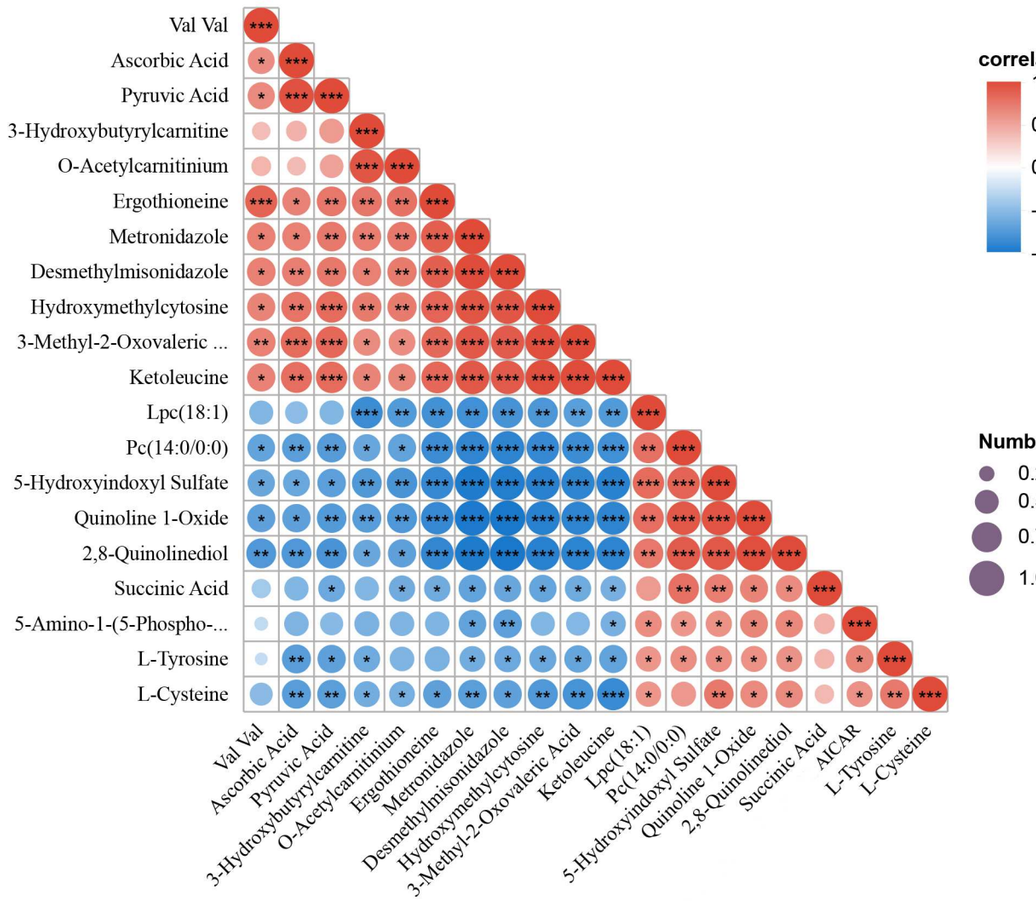
E

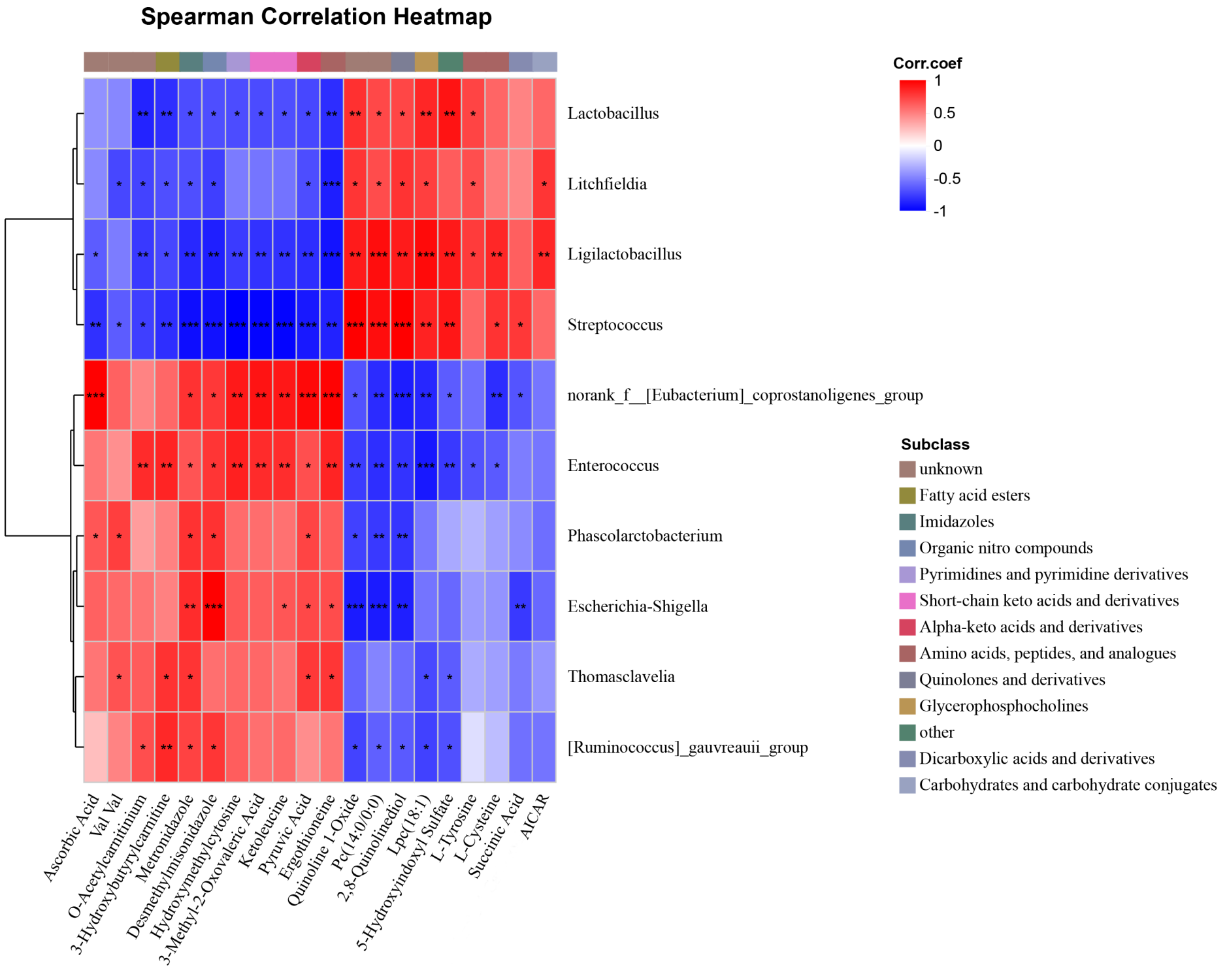

Expression Profile & VIP of Metabolites
Ascorbic Acid
O-Acetylcarnitinium
3-Hydroxybutyrylcarnitine
Val Val
Pyruvic Acid
Metronidazole
Desmethylmisonidazole
Ergothioneine
Hydroxymethylcytosine
3-Methyl-2-Oxovaleric Acid
Ketoleucine
L-Cysteine
5-Amino-1-(5-Phospho-D-Ribosyl)Imidazole-4-Carboxylic Acid
L-Tyrosine
Succinic Acid
Quinoline 1-Oxide
5-Hydroxyindoxyl Sulfate
2,8-Quinolinediol
Pc(14:0/0:0)
Lpc(18:1)
Control
Antibiotic
VIP
-log(p_value)

F


KEGG Enrichment Analysis(Antibiotic_vs_Control)
Lysine degradation
D-Amino acid metabolism
Phenylalanine metabolism
Aminoacyl-tRNA biosynthesis
Valine, leucine and isoleucine biosynthesis
Histidine metabolism
Alanine, aspartate and glutamate metabolism
beta-Alanine metabolism
Ascorbate and aldarate metabolism
Nucleotide metabolism
Pyrimidine metabolism
Efferocytosis
Purine metabolism
Arginine and proline metabolism
Glycine, serine and threonine metabolism
Pantothenate and CoA biosynthesis
Thiamine metabolism
Glyoxylate and dicarboxylate metabolism
ABC transporters
Cysteine and methionine metabolism
P_value
Number

G


Val Val
Ascorbic Acid
Pyruvic Acid
3-Hydroxybutyrylcarnitine
O-Acetylcarnitinium
Ergothioneine
Metronidazole
Desmethylmisonidazole
Hydroxymethylcytosine
3-Methyl-2-Oxovaleric ...
Ketoleucine
Lpc(18:1)
Pc(14:0/0:0)
5-Hydroxyindoxyl Sulfate
Quinoline 1-Oxide
2,8-Quinolinediol
Succinic Acid
5-Amino-1-(5-Phospho-...
L-Tyrosine
L-Cysteine
AICAR
correlation
Number


Spearman Correlation Heatmap
Corr.coef
1
0.5
0
-0.5
-1
Lactobacillus
Litchfieldia
Ligilactobacillus
Streptococcus
norank_f__[Eubacterium]_coprostanoligenes_group
Enterococcus
Phascolarctobacterium
Escherichia-Shigella
Thomasclavelia
[Ruminococcus]_gauvreauii_group
Ascorbic Acid
Val Val
O-Acetylcarnitinium
3-Hydroxybutyrylcarnitine
Metronidazole
Desmethylmisonidazole
Hydroxymethylcytosine
3-Methyl-2-Oxovaleric Acid
Ketoleucine
Pyruvic Acid
Ergothioneine
Quinoline 1-Oxide
Pc(14:0/0:0)
2,8-Quinolinediol
Lpc(18:1)
5-Hydroxyindoxyl Sulfate
L-Tyrosine
L-Cysteine
Succinic Acid
AICAR
Subclass
unknown
Fatty acid esters
Imidazoles
Organic nitro compounds
Pyrimidines and pyrimidine derivatives
Short-chain keto acids and derivatives
Alpha-keto acids and derivatives
Amino acids, peptides, and analogues
Quinolones and derivatives
Glycerophosphocholines
other
Dicarboxylic acids and derivatives
Carbohydrates and carbohydrate conjugates

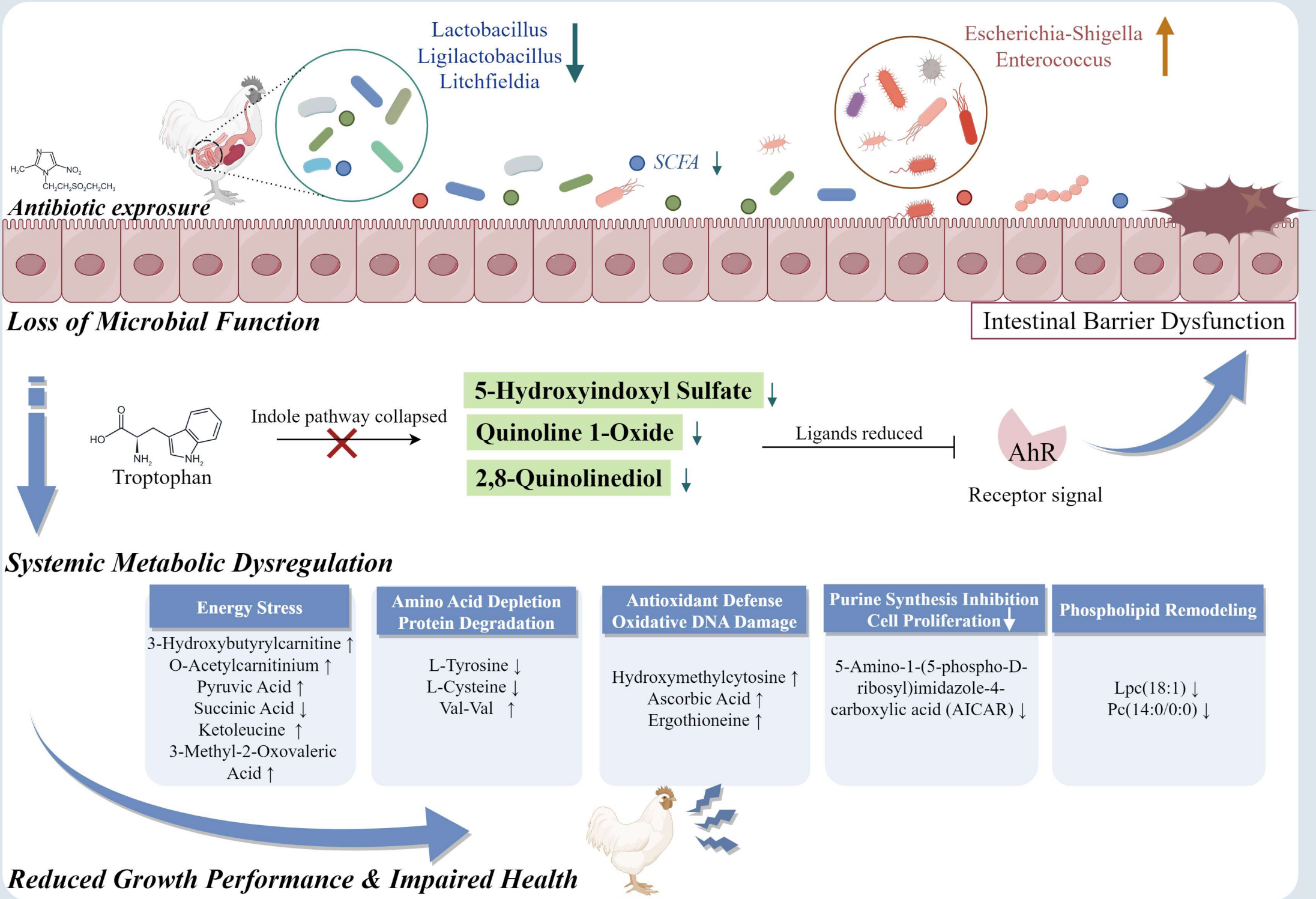

Lactobacillus
Ligilactobacillus
Litchfieldia
Escherichia-Shigella
Enterococcus
SCFA
Antibiotic exprosure
Loss of Microbial Function
Intestinal Barrier Dysfunction
Troptophan
Indole pathway collapsed
5-Hydroxyindoxyl Sulfate
Quinoline 1-Oxide
2,8-Quinolinediol
Ligands reduced
AhR
Receptor signal
Systemic Metabolic Dysregulation
Energy Stress
3-Hydroxybutyrylcarnitine ↑
O-Acetylcarnitinium ↑
Pyruvic Acid ↑
Succinic Acid ↓
Ketoleucine ↑
3-Methyl-2-Oxovaleric Acid ↑
Amino Acid Depletion Protein Degradation
L-Tyrosine ↓
L-Cysteine ↓
Val-Val ↑
Antioxidant Defense Oxidative DNA Damage
Hydroxymethylcytosine ↑
Ascorbic Acid ↑
Ergothioneine ↑
Purine Synthesis Inhibition Cell Proliferation
5-Amino-1-(5-phospho-D-ribosyl)imidazole-4-carboxylic acid (AICAR) ↓
Phospholipid Remodeling
Lpc(18:1) ↓
Pc(14:0/0:0) ↓
Reduced Growth Performance & Impaired Health

Table 1 Intestinal and organ indices of antibiotic-treated broilers.

Item	Day	Control	Antibiotic	P-value
Intestinal length, cm				
Duodenum	14	21.50 ± 0.74	20.75 ± 0.90	0.370
	21	22.40 ± 0.51	23.20 ± 0.58	0.332
	35	31.00 ± 1.29	26.60 ± 0.51	0.011*
Jejunum	14	77.20 ± 0.73	71.00 ± 2.08	0.018*
	21	76.40 ± 3.66	72.40 ± 1.33	0.434
	35	88.00 ± 3.31	81.20 ± 4.22	0.361
Ileum	14	6.80 ± .0.74	7.50 ± 0.48	0.385
	21	10.00 ± 0.35	7.90 ± 0.24	0.001***
	35	10.50 ± 0.34	10.50 ± 0.22	1.000
Cecum	14	7.50 ± 0.78	7.25 ± 0.32	0.644
	21	9.00 ± 0.57	8.58 ± 0.47	0.584
	35	1.00 ± 0.45	10.83 ± 0.29	0.862
Colorectum	14	3.00 ±0.16	2.25 ± 0.25	0.033*
	21	3.20 ± 0.25	3.08 ± 0.27	0.761
	35	10.50 ± 0.21	10.50 ± 0.41	0.179
Organ index, %				
Thymus	14	0.196 ± 0.03	0.159 ± 0.02	0.344
	21	0.181 ± 0.02	0.154 ± 0.01	0.291
	35	0.201 ± 0.01	0.149 ±0.05	0.025*
Spleen	14	0.080 ± 0.42	0.081 ± 0.23	0.979
	21	0.094 ±0.51	0.047 ± 0.28	0.018*
	35	0.322 ± 0.03	0.173 ± 0.03	0.014*
Bursa of Fabricius	14	0.138 ± 0.01	0.114 ± 0.12	0.265
	21	0.191 ± 0.22	0.167 ± 0.01	0.748
	35	0.221 ± 0.03	0.190 ± 0.21	0.212
Liver	14	2.325 ± 0.13	2.398 ± 0.09	0.675
	21	2.074 ± 0.07	1.987 ± 0.37	0.403
	35	2.805 ± 0.13	2.219 ± 0.17	0.019*
Heart	14	0.574 ± 0.08	0.456 ± 0.02	0.283
	21	0.638 ± 0.06	0.492 ± 0.12	0.028*
	35	0.718 ±0.17	0.595 ± 0.01	0.073
Pancreas	14	0.391 ± 0.05	0.274 ± 0.12	0.094
	21	0.259 ± 0.24	0.239 ± 0.31	0.224
	35	0.238 ± 0.02	0.177 ±0.14	0.007**
Kidney	14	0.325 ±0.32	0.264 ± 0.17	0.028*
	21	0.277 ±0.31	0.265 ± 0.02	0.340
	35	0.364 ± 0.02	0.334 ±0.01	0.130

Abbreviations: Control group (basal diet); Antibiotic group (basal diet + antibiotic). P-values were

calculated using independent samples t-test.*P < 0.05, **P < 0.01, ***P < 0.001.